This article was downloaded by: [University of Lethbridge]
On: 28 July 2015, At: 16:49
Publisher: Taylor & Francis
Informa Ltd Registered in England and Wales Registered Number: 1072954 Registered office: 5 Howick Place, London, SW1P 1WG

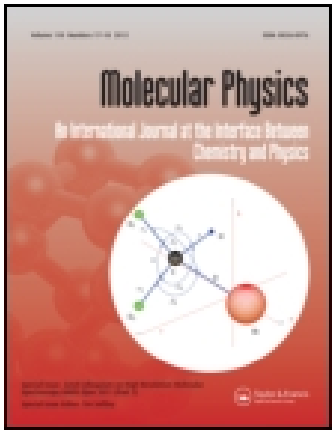

Molecular Physics: An International Journal at the Interface Between Chemistry and Physics
Publication details, including instructions for authors and subscription information:
http://www.tandfonline.com/loi/tmph20

Experimental and theoretical study of N_2-broadened acetylene line parameters in the $\nu_1+\nu_3$ band over a range of temperatures

Hoimonti Rozario [a] , Jolene Garber [a] , Chad Povey [a] , Daniel Hurtmans [b] , Jeanna Buldyreva [c] & Adriana Predoi-Cross [a]

[a] Alberta Terrestrial Imaging Centre, Department of Physics and Astronomy , University of Lethbridge , 4401 University Drive, Lethbridge , AB , T1K 3M4 Canada

[b] Service de Chimie Quantique et Photophysique CP 160/09 , Université Libre de Bruxelles , 50, Av. Roosevelt, B-1050 Bruxelles , Belgium

[c] Institut UTINAM UMR CNRS 6213, Université de Franche-Comté , 16 Route de Gray, 25030 Besançon cedex , France

Published online: 18 Sep 2012.

To cite this article: Hoimonti Rozario , Jolene Garber , Chad Povey , Daniel Hurtmans , Jeanna Buldyreva & Adriana Predoi-Cross (2012) Experimental and theoretical study of N_2-broadened acetylene line parameters in the $\nu_1+\nu_3$ band over a range of temperatures, Molecular Physics: An International Journal at the Interface Between Chemistry and Physics, 110:21-22, 2645-2663, DOI: 10.1080/00268976.2012.720040

To link to this article: http://dx.doi.org/10.1080/00268976.2012.720040

PLEASE SCROLL DOWN FOR ARTICLE

Taylor & Francis makes every effort to ensure the accuracy of all the information (the "Content") contained in the publications on our platform. However, Taylor & Francis, our agents, and our licensors make no representations or warranties whatsoever as to the accuracy, completeness, or suitability for any purpose of the Content. Any opinions and views expressed in this publication are the opinions and views of the authors, and are not the views of or endorsed by Taylor & Francis. The accuracy of the Content should not be relied upon and should be independently verified with primary sources of information. Taylor and Francis shall not be liable for any losses, actions, claims, proceedings, demands, costs, expenses, damages, and other liabilities whatsoever or howsoever caused arising directly or indirectly in connection with, in relation to or arising out of the use of the Content.

This article may be used for research, teaching, and private study purposes. Any substantial or systematic reproduction, redistribution, reselling, loan, sub-licensing, systematic supply, or distribution in any form to anyone is expressly forbidden. Terms & Conditions of access and use can be found at http://www.tandfonline.com/page/terms-and-conditions

Molecular Physics
Vol. 110, Nos. 21–22, November 2012, 2645–2663

Taylor & Francis
Taylor & Francis Group

SPECIAL ISSUE: FASE (FEMTO-, ASTRO-, SPECTRO-ETHYNE)

Experimental and theoretical study of N_2-broadened acetylene line parameters in the $\nu_1 + \nu_3$ band over a range of temperatures

Hoimonti Rozario[a], Jolene Garber[a], Chad Povey[a], Daniel Hurtmans[b], Jeanna Buldyreva[c] and Adriana Predoi-Cross[a]*

[a]*Alberta Terrestrial Imaging Centre, Department of Physics and Astronomy, University of Lethbridge, 4401 University Drive, Lethbridge, AB, T1K 3M4 Canada;* [b]*Service de Chimie Quantique et Photophysique CP 160/09, Université Libre de Bruxelles, 50, Av. Roosevelt, B-1050 Bruxelles, Belgium;* [c]*Institut UTINAM UMR CNRS 6213, Université de Franche-Comté, 16 Route de Gray, 25030 Besançon cedex, France*

(*Received 30 May 2012; final version received 6 August 2012*)

N_2-broadened line widths and N_2-pressure induced line shifts have been measured for transitions in the $\nu_1 + \nu_3$ band of acetylene at seven temperatures in the range 213–333 K to obtain the temperature dependences of broadening and shift coefficients. For the room-temperature spectra the line mixing effects have been also investigated. The Voigt and hard-collision line profile models were used to retrieve the line parameters. All spectra were recorded using a 3-channel tuneable diode laser spectrometer. The line-broadening and line-shifting coefficients as well as their temperature-dependence parameters have been also evaluated theoretically, in the frame of a semi-classical approach based on an exponential representation of the scattering operator, an intermolecular potential composed of electrostatic quadrupole–quadrupole and pairwise atom–atom interactions as well as on exact trajectories driven by an effective isotropic potential.

Keywords: acetylene; N_2-pressure broadening; N_2-pressure-induced shifts; spectral line shape; infrared spectroscopy; spectral line parameters; semi-classical calculations

Downloaded by [University of Lethbridge] at 16:49 28 July 2015

1. Introduction

Infrared remote sensing has long been used to learn about the composition and structure of planetary atmospheres [1]. Spectra of the outer planets and their moons have been recorded by various instruments at ground-based telescopes, on aircraft and on spacecraft. To properly interpret these telescope and spacecraft observations, particularly for atmospheres that have compositions, temperature and pressure regimes quite different from those in the terrestrial atmosphere, laboratory studies are required.

The atmosphere of the giant planets and that of Titan contains acetylene as a trace constituent playing an active role in their atmospheric chemistry. Acetylene is known to be a trace constituent of Earth's atmosphere as well, being produced by chemical reactions in the atmosphere itself and by hydrocarbon flames.

Due to the importance of this molecular species, good models for its spectral line shapes broadened by air, nitrogen, and hydrogen (N_2 for the Titan and Earth atmospheres, H_2 for those of Jupiter and Saturn), are required for accurate retrievals of its concentration profiles. The spectroscopic line shape parameters are needed as functions of pressure, quantum number, and temperature.

That is why numerous spectroscopic line shape studies [2–19] have focused on self- or foreign-broadened line parameters of acetylene. Moreover, since at elevated gas pressures the overlapping of spectral lines causes significant deviation of the spectral profiles from independently additive superposition of Lorentzian line shapes, the line mixing effects have been also investigated. For sub-atmospheric pressures these effects have been observed and quantified for transitions in the $\nu_1 + \nu_5$ Q-branches of $\Pi \leftarrow \Sigma$ symmetry [6] as well as in the $\nu_4 + \nu_5 - \nu_4$ and $2\nu_5 - \nu_5$ Q-branches of $\Sigma \leftarrow \Pi$ symmetry at room [9] and low [10] temperatures. Broadening coefficients obtained from semi-classical calculations based on the Robert–Bonamy (RB) formalism employing parabolic trajectories [4,7] or on the Energy Corrected Sudden (ECS) formalism [9,10] have been compared with experimental results with good agreement. A summary of previous spectroscopic line shape studies on acetylene is presented in Table 1.

The ν_5 band is the most studied band at room [3,4,7] and low [5,8] temperatures. The spectral profiles

*Corresponding author. Email: Adriana.predoicross@uleth.ca

ISSN 0026–8976 print/ISSN 1362–3028 online
© 2012 Taylor & Francis
http://dx.doi.org/10.1080/00268976.2012.720040
http://www.tandfonline.com

Table 1. Summary of previous studies of acetylene lines broadened by N_2.

Vibrational Band	Temp.	Broadener	Assignment range	Line shape model	Ref.
ν_5	297 K	N_2, O_2	P(29)–R(25)	Voigt	[3]
ν_5	297 K	N_2, O_2	P(35)–R(34)	Theoretical (RB)	[4]
ν_5	147–295 K	H_2, N_2, He, Ar	P(8)–R(21)	Voigt	[5]
ν_5	296 K	H_2, N_2, He, Ar	R(3)–R(34)	Theoretical (RB)	[7]
ν_5	173.4 K	N_2	P(29)–R(28)	Rautian, theoretical (RB)	[8]
$\nu_4+\nu_5-\nu_4$	296 K	N_2, He	Q(1)–Q(35)	Theoretical (ECS)	[9]
$2\nu_5-\nu_5$	296 K	N_2, He	Q(1)–Q(35)	Theoretical (ECS)	[9]
$\nu_4+\nu_5-\nu_4$	183.2,198.2 K	N_2, He	Q(1)–Q(35)	Theoretical (ECS)	[10]
$2\nu_5-\nu_5$	183.2,198.2 K	N_2, He	Q(1)–Q(35)	Theoretical (ECS)	[10]
$\nu_4+\nu_5$	296 K	N_2, air	P(31)–R(20)	Voigt	[2]
$\nu_4+\nu_5$	173.2–273.2 K	N_2	P(1)–R(23)	Voigt, Rautian	[13]
$\nu_4+\nu_5$	298 K	N_2	P(17)–R(22)	Voigt, Rautian	[14]
$\nu_4+\nu_5$	173.2–298.2 K	N_2	R(11)–P(23)	Voigt, Rautian, Galatry	[15]
$\nu_1+\nu_3$	295 K	H_2, N_2, D_2, air	P(31)–R(27)	Voigt	[12]
$\nu_1+\nu_3$	296 K	C_2H_2, N_2	P(11)	Voigt, Rautian, Galatry	[16]
$\nu_1+\nu_3$	195, 373, 473 K	N_2	P(25)–R(25)	Voigt	[18]
$\nu_1+\nu_3$	296 K	C_2H_2, N_2,O_2, CO_2	P(22)–P(26)	Voigt	[19]
$\nu_1+\nu_5$	296 K	C_2H_2, N_2, Ar	R(0)–R(7),Q(7)–Q(29)	Rautian	[6]
$\nu_1+3\nu_3$	298 K	N_2, O_2,He, Ar, Ne, Kr, Xe	P(17)–R(22)	Galatry, Rautian	[11]

Downloaded by [University of Lethbridge] at 16:49 28 July 2015

have been modelled using either the Voigt [3,5] or Rautian profiles [8]. The experimental N_2-broadening coefficients have been compared with theoretical semi-classical N_2-broadening coefficients [4,7,8].

The $\nu_4+\nu_5$ combination band has been studied at room [2,14] and low temperatures [13,15] using tunable diode laser spectroscopy. The line parameters have been modeled using the Voigt profile [2,13–15] as well as the Rautian (hard-collision) and Galatry (soft-collision) models [13–15] which take into account the collisional narrowing of spectral lines due to molecular confinement.

The $\nu_1+\nu_3$ band is a strong combination band often used as a near-infrared frequency calibration standard. Transitions from this band have been modeled with the Voigt [12,16,18,19], Rautian and Galatry profiles [16]. Spectra were recorded at room temperature [12, 16] and at 195 K, 373 K, 473 K [18] providing the authors with measurements of the N_2-broadening and N_2-shift coefficients. Transitions in the $\nu_1+3\nu_3$ band broadened by N_2, O_2, air, He, Ar, Ne, Kr, Xe were studied in Ref. [11] using diode-laser spectroscopy and the profile models of Galatry and Rautian. The authors were also able to deduce effective friction coefficients from measured narrowing parameters for acetylene mixed with foreign gases. Minutolo *et al*. [19] measured five *P*-branch transitions in the $\nu_1+\nu_3$ band broadened by C_2H_2, N_2, O_2, CO_2 using a diode laser spectrometer. The self- and foreign-broadening coefficients were retrieved using a Voigt model. A recent study of self-broadened transitions in the $\nu_1+\nu_2+\nu_4+\nu_5$ band over a wide range of temperatures [17] was the first one to take into account the effects of molecular speed dependence on broadening coefficients.

In the present extensive study, a 3-channel tuneable diode laser described in Ref. [17] was used to record the spectra at different temperatures and pressures in order to deduce the N_2-broadened acetylene line widths and shifts as well as their temperature dependences for *P*- and *R*-branch transitions in the $\nu_1+\nu_3$ band. Theoretical estimation of line broadening and shift coefficients was performed by a semi-classical approach of Robert–Bonamy type involving exact classical trajectories governed by the isotropic potential. Since this isotropic trajectory approximation is not very well justified for the long polyatomic molecule C_2H_2 [20–22], the previous calculations on the C_2H_2–N_2 system [23] were improved by the use of an 'effective' isotropic potential.

2. Experimental details and line shape analysis

The 3-channel diode laser spectrometer used in the present study is described in detail in Ref. [17]; we recall here only its main features. The first channel contains a temperature- and pressure-controlled cell of 1.47 m optical path. The second channel contains a room-temperature reference cell of 1.5 m optical path, filled with acetylene at low pressure and allowing accurate measurements of pressure shifts. The third channel records the background of the laser system. Three InGas detectors monitor the optical signals on

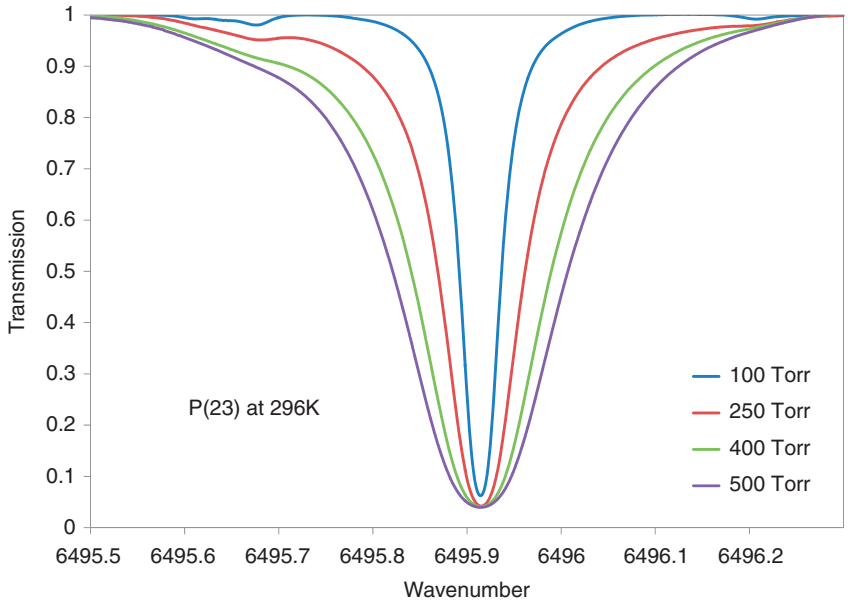

Figure 1. Room-temperature spectra recorded for the $P(23)$ transition of the $\nu_1 + \nu_3$ band of C_2H_2 broadened by N_2.

Downloaded by [University of Lethbridge] at 16:49 28 July 2015

the three spectrometer channels. The wavelength is measured using a combination of a Fabry-Perot cavity and a WA-1500 EXFO Wavemeter. The entire experimental setup is controlled and monitored using Labview software. Owing to high signal-to-noise ratio provided by the data acquisition system (better than 2000 in the 1500 to 1570 nm range) this setup enables very accurate line shape measurements and fundamental spectroscopic studies of molecular interactions.

The mixture of acetylene and nitrogen with a quoted concentration of 9.94% acetylene was supplied by Praxair. Tests on the P(11) transition showed that the concentration was within 0.5% from the quoted value. The pressures were measured using two MKS Baratron gauges with full scale readings of 10 and 1000 Torr. The temperatures were monitored with five platinum resistor thermometers mounted at different locations inside the temperature-controlled cell and a Lakeshore temperature sensor monitor. The temperature stability along the cell was within 0.3 K [17] at all studied temperatures (from 213 to 333 K with an increment of 20 K).

The measurements have been performed for 47#*P*- and *R*- transitions in the $\nu_1 + \nu_3$ band of acetylene. For every set temperature, spectra were recorded at four different pressures, namely 100, 250, 400 and 500 Torr. A sample of these spectra is presented in Figure 1 for the $P(23)$ transition at room temperature.

The spectral lines were modeled using a multispectral software [24] that convolves the instrumental line shape [25] with the line shape of choice (Voigt, Rautian, Galatry) and adjusts the individual line parameters by minimizing the difference between the experimental and modeled spectra with a Marquardt algorithm.

The recorded line positions were internally calibrated using the data listed within the HITRAN 2008 database [26]. In our analyses with the Voigt and Rautian profiles we have used the values form Ref. [26] as initial guesses for the fit parameters. The narrowing parameter was set at the value quoted in Ref. [16].

The N_2-broadening ($\gamma^0_{N_2}$) and pressure-shift ($\delta^0_{N_2}$, δ'_{N_2}, δ'_{1N_2}, δ'_{2N_2}) coefficients (in $cm^{-1}\,atm^{-1}$) were determined by the following expressions:

$$\gamma(p,T) = \left[p \times \gamma^0_{N_2}(p_0,T_0) \times (1-\chi) \times \left(\frac{T_0}{T}\right)^n + \gamma^0_{self}(p_0,T_0) \times \chi \times \left(\frac{T_0}{T}\right)^n\right], \quad (1)$$

$$\nu(T) = \nu_0 + p \times [\delta^0_{N_2}(T) \times (1-\chi) + \delta^0_{self}(T) \times \chi], \quad (2)$$

$$\delta^0_{N_2}(T) = \delta^0_{N_2}(T_0) + \delta'_{N_2} \times (T - T_0), \quad (3)$$

$$\delta^0_{N_2}(T) = \delta^0_{N_2}(T_0) + \delta'_{1N_2} \times (T - T_0) + \delta'_{2N_2} \times (T - T_0)^2/2. \quad (4)$$

Downloaded by [University of Lethbridge] at 16:49 28 July 2015

In Equation (1) $\gamma(p,T)$ is the half-width (in cm^{-1}) of the spectral line at total sample pressure $p = p_{N_2} + p_{self}$ (in atm) and temperature T (in Kelvin), χ is the ratio of p_{self} to p, the reference pressure p_0 corresponds to 1 atm, and the reference temperature T_0 is 296 K. Equation (2) gives the measured line position $\nu(T)$ as a function of the position ν_0 at zero pressure and the total pressure p, with the temperature dependence of shift coefficients modeled by either Equation (3) or Equation (4). The self-broadening and self-shift coefficients are taken from Ref. [26].

To account for the line-mixing effects within the individual transitions considered in the present work we have used (weak) line mixing coefficient Y_{0i} calculated by the Exponential Power Gap method of Ref. [17]. The total calculated line mixing component, Y_i, and the total sample pressure p are related by the expression $Y_i = pY_{0i}$. The parameter β used to express the off-diagonal matrix elements as a function of the collisional transfer rate was $\beta = 0.56$. The Exponential Power gap (EPG) law calculates the collisional transfer rates from the lower rotational level k to a higher rotational level j as given by Equation (15) of Ref. [17]. Parameters a, b, and c were optimized so that the calculated broadening coefficients matched the experimental ones. For values retrieved for P-branch transitions the parameters were: $a = 0.06184$, $b = 0.31698$, $c = 1.28210$, and for R-branch transitions they were: $a = 0.06883$, $b = 0.37615$, $c = 1.17421$. For each column of the relaxation matrix, the sum of off-diagonal elements of the relaxation matrix matches the measured pressure broadening coefficients through the sum rule within 1.54×10^{-23} for P-branch transitions and 1.70×10^{-22} for R-branch transitions. The calculated asymmetry due to line mixing has been taken into account in our non-linear fitting procedure supposing that the temperature dependence of the weak line mixing coefficients is negligible. The retrieved broadening coefficients are not affected by the inclusion of line mixing effects. However, the pattern of the shifts as a function of m is smoother when line mixing is accounted for.

3. Semi-classical formalism for line broadening and shift calculations

Semi-classical calculations of line widths γ and line shifts δ have been performed with the standard expression of the perturbative approach of Robert and Bonamy [27] but supplied by exact trajectories governed by the isotropic part of the intermolecular interaction potential [28]. For the considered vibrotational transition $i \to f$ these line widths and shifts (in cm^{-1}) can be written as

$$\gamma_{fi} - i\delta_{fi} = \frac{n\bar{v}}{2\pi c}\int_0^\infty 2\pi b db \left\langle 1 - e^{-\mathrm{Re}\, S_2} e^{-i(\mathrm{Im}\, S_2 + S_1)} \right\rangle_{J_2}, \tag{5}$$

where n is the number density of perturbing particles, $\bar{v}$ is the mean thermal velocity, b is the impact parameter further replaced by the distance of the closest approach r_c, S_1 and S_2 are, respectively, the first- and second-order contributions to the scattering matrix, and $\langle \cdots \rangle_{J_2}$ means the average over the rotational states of the perturber. It has been shown in the frame of quantum-mechanical close coupling calculations [29] that for the C_2H_2–N_2 system the approximation of the mean thermal velocity is accurate for the temperatures above 143 K. Therefore we expect that this approximation is also valid for the present system.

The explicit form of Re S_2 term for two linear molecules following exact trajectories can be either deduced from the general formulae for two asymmetric colliders 1 and 2 [30] or calculated directly from the rotationally invariant representation of the intermolecular interaction potential

$$V(1,2,\vec{r}) = \sum_{l_1 l_2 l} V_{l_1 l_2 l}(r) \sum_{m_1 m_2 m} C^{lm}_{l_1 m_1 l_2 m_2} Y_{l_1 m_1}(\theta_1, \varphi_1) \times Y_{l_2 m_2}(\theta_2, \varphi_2) C^*_{lm}(\theta, \varphi) \tag{6}$$

(the corresponding imaginary part Im S_2 is further obtained with Equation (10) of Ref. [27]). In Equation (6) the products of spherical harmonics $Y_{l_1 m_1}(\theta_1, \varphi_1) \times Y_{l_2 m_2}(\theta_2, \varphi_2) C^*_{lm}(\theta, \varphi)$ represent the rotationally invariant basis in the laboratory-fixed frame (the asterisk means the complex conjugation), $C^{lm}_{l_1 m_1 l_2 m_2}$ are the Clebsch–Gordan coefficients and $V_{l_1 l_2 l}(r)$ are the radial potential components including contributions from various kinds of intermolecular interactions. In the present work we have considered $l_1 \le 2$ and $l_2 \le 2$ and composed the potential as a sum of electrostatic (e) quadrupole–quadrupole and pairwise atom–atom (a) interactions. For the electrostatic term $V^e_{224}(r) = 4\pi\sqrt{70} Q_1 Q_2 / (5r^5)$ the quadrupole moment values $Q_{C2H2} = 4.0 \times 10^{-26}$ esu cm^2 [8] and $Q_{N2} = -1.52 \times 10^{-26}$ esu cm^2 [31] (for final calculations) have been used. For the atom–atom terms the radial potential components are functions of the interatomic parameters d_{ij} and e_{ij} (defined via the Lennard–Jones parameters ε_{ij}, σ_{ij} of the atoms i and j as $d_{ij} = 4\varepsilon_{ij}\sigma^{12}_{ij}$, $e_{ij} = 4\varepsilon_{ij}\sigma^6_{ij}$):

$$V^a_{l_1 l_2 l}(r) = \sum_{i,j} \left[d_{ij} f^{12}_{l_1 l_2 l}(r_{1i}, r_{2j}, r) - e_{ij} f^6_{l_1 l_2 l}(r_{1i}, r_{2j}, r) \right] \xi_{1i} \xi_{2j}, \tag{7}$$

Table 2. Atom–atom interaction parameters for the C_2H_2–N_2 system.

r_{1i}, r_{2j} (Å) [8]		d_{ij} 10^{-7} erg Å^{12}	e_{ij} 10^{-10} erg Å^6	Reference	V_{iso} model
$r_{1C}=0.6035$	CN	0.3234	0.2922	[33]	"V_{iso} LJ"
	HN	0.0571			"numerical V_{iso}"
					"V_{iso} LJ trial"
$r_{1H}=1.6614$	CN	0.0018	0.0803		
	HN	0.0002	0.0146	calculated from [34] ("final" values)	"numerical V_{iso}–2"
$r_{2N}=0.550$	CN	0.4773	0.0004		
	HN	0.0571	0.2983	calculated from [34] ("initial" CN values)	"numerical V_{iso}–3"
			0.0803		

where $\xi_{1i}=1$ for the atom i having a positive z-value in the molecular frame and $\xi_{1i}=(-1)^{l_1}$ for the atom i with a negative z-value (the molecular z-axis is chosen along the molecular symmetry axis and the origin is taken at the molecular center of mass); similar definitions of ξ_{2j} are applied for the j-atoms of the perturbing molecule. The functions $f^n_{l_1l_2l}(r_{1i},r_{2j},r)$ come from the two-centre expansion [32] of the interatomic distances $r^{-n}_{1i,2j}$ and for the chosen representation of the intermolecular potential have the form:

$$f^n_{l_1l_2l}(r_{1i},r_{2j},r) = \frac{(-1)^{l_2}}{r^n}4\pi\sqrt{(2l_1+1)(2l_2+1)}C^{l0}_{l_10l_20}\sum_{p,q}\left(\frac{r_{1i}}{r}\right)^p\left(\frac{r_{2j}}{r}\right)^q \times\frac{(n+p+q-l-3)!!(n+p+q+l-2)!!}{(n-2)!(p-l_1)!!(p+l_1+1)!!(p-l_1)!!(p+l_1+1)!!} \times\left\{1+\delta_{n1}(\delta_{pl_1}\delta_{ql_2}\delta_{p+q,l_1}-1)\right\} \quad (8)$$

with $p=l_1,\ l_1+2,\ l_1+4,\ldots;\ q=l_2,\ l_2+2,\ l_2+4,\ldots$. The sets of atom–atom parameters tested in the present work are gathered in Table 2.

With the potential of Equation (6) the real part of the second-order contribution composed of three terms $S_{2,i2}$, $S_{2,f2}$, $S_{2,f2i2}$ is given by:

$$S_{2,i2}=\frac{2r_c^2}{\hbar^2\bar{v}^2}\sum_{l_1l_2l}\sum_{J_i'J_2'}\left(C^{J_i'0}_{J_i0l_10}\right)^2\left(C^{J_2'0}_{J_20l_20}\right)^2 f_{l_1l_2l}, \quad (9)$$

$$S_{2,f2i2}=-\frac{2r_c^2}{\hbar^2\bar{v}^2}\sum_{l_1l_2l}(-1)^{\rho+l_2+l}D\left(J_iJ_f;\,\rho l_1\right) \times\sum_{J_2'}\left(C^{J_2'0_2}_{J_20l_20}\right)^2 f_{l_1l_2l}; \quad (10)$$

the coefficients $D(J_iJ_f;\ \rho l_1)=(-1)^{J_i+J_f}2[(2J_i+1)\times(2J_f+1)]^{1/2}(C^{J_i0}_{J_i0l_10})(C^{J_f0}_{J_f0l_10})W(J_iJ_fJ_iJ_f;\,\rho l_1)$ are defined in particular by the Racah coefficients $W(J_iJ_fJ_iJ_f;\,\rho l_1)$; $\rho=1$ for the infrared absorption. The so-called resonance functions $f_{l_1l_2l}$ have two arguments (for a given temperature): the distance of the closest approach r_c and the resonance parameter $k_c=\omega r_c/\bar{v}$:

$$f_{l_1l_2l}=\sum_m\frac{(l-m)!(l+m)!}{2^{2l}((l-m)/2)!^2((l+m)/2)!^2} \times\left|\int_1^\infty\frac{\left\{\begin{array}{l}\mathrm{d}y V_{l_1l_2l}(r_cy)\,y\cos[k_cA_0(y)\\ +m\sqrt{1-V^\circ_{iso}(r_c)}A_2(y)]\end{array}\right\}}{\sqrt{y^2-1+V^\circ_{iso}(r_c)-y^2V^\circ_{iso}(yr_c)}}\right|^2. \quad (11)$$

They contain the integration over exact classical trajectories with the dimensionless integration variable $y=r/r_c$ and depend on the reduced isotropic potential $V^\circ_{iso}=2V_{iso}/(m^\circ\bar{v}^2)$ (m° is the reduced mass of the molecular pair), and on the integrals $A_n(y)=\int_1^y \mathrm{d}z\,z^{-n+1}[z^2-1+V^\circ_{iso}(r_c)-z^2V^\circ_{iso}(zr_c)]^{-1/2}$.

For the line-width calculations, the contributions coming from the imaginary part of S_2 (non-commutative character of interaction at two different times) and from S_1 (vibrational dependence of the isotropic potential) are very small and have been neglected in the present work. The term S_1 yields, however, the dominant vibrational contribution to the pressure-induced shift of spectral lines, as is shown below.

To govern the trajectories, the isotropic potential can be chosen in an analytical (e.g. Lennard–Jones 12-6) form or in an accurate numerical form computed from the sum of atom–atom interactions. In the first case the Jacobian for the change of variables $bdb\to r_cdr_c$ in Equation (5) has an analytical form and is defined only by the Lennard–Jones parameters ε and σ (see [27]). In the second case the values of the first derivative of the isotropic potential are additionally required: $bdb=r_cdr_c[1-V^\circ_{iso}(r_c)-(r_c/2)(\mathrm{d}V^\circ_{iso}(r)/\mathrm{d}r)\big|_{r=r_c}]$ and are obtained by numerical derivation for the purposes of the present work. Since the calculated line-shape parameters are very sensitive to the characteristics of V_{iso} we have tested several models: first, the standard Lennard–Jones 12-6 form [33] ($\varepsilon=131.1$ K, $\sigma=4.0135$ Å) named 'V_{iso} LJ', then

Downloaded by [University of Lethbridge] at 16:49 28 July 2015

the numerical potentials computed as the isotropic part of the atom–atom interactions with the atom–atom parameters listed in Table 2; these models of V_{iso} are shown in Figure 2(a). However, none of these isotropic potentials have led to an accurate prediction of room-temperature line broadening coefficients for all values of the rotational quantum number (Figure 3(a)). Such a difficulty of semi-classical approaches to estimate the collisional line broadening for C_2H_2 has been already observed previously and ascribed to a non-validity of the rotation–translation decoupling for long anisotropic molecules [20–22]. We have attempted therefore to find further some kind of 'effective' isotropic potential giving a realistic prediction of line widths. Namely, given the fact that at high J-values the line widths are mainly due to the short-range atom–atom interactions, we have tried to decrease the contributions from these terms by keeping the same potential depth[1] $\varepsilon = 131.1\,\mathrm{K}$ and increasing progressively the Lennard-Jones parameter σ (see Figure 2(b)): $\sigma = 4.2\,\text{Å}$ ('Viso LJ trial-I' curve), $\sigma = 4.4\,\text{Å}$ ('Viso LJ trial-II' curve), $\sigma = 4.5\,\text{Å}$ ('Viso LJ trial-IV' curve);

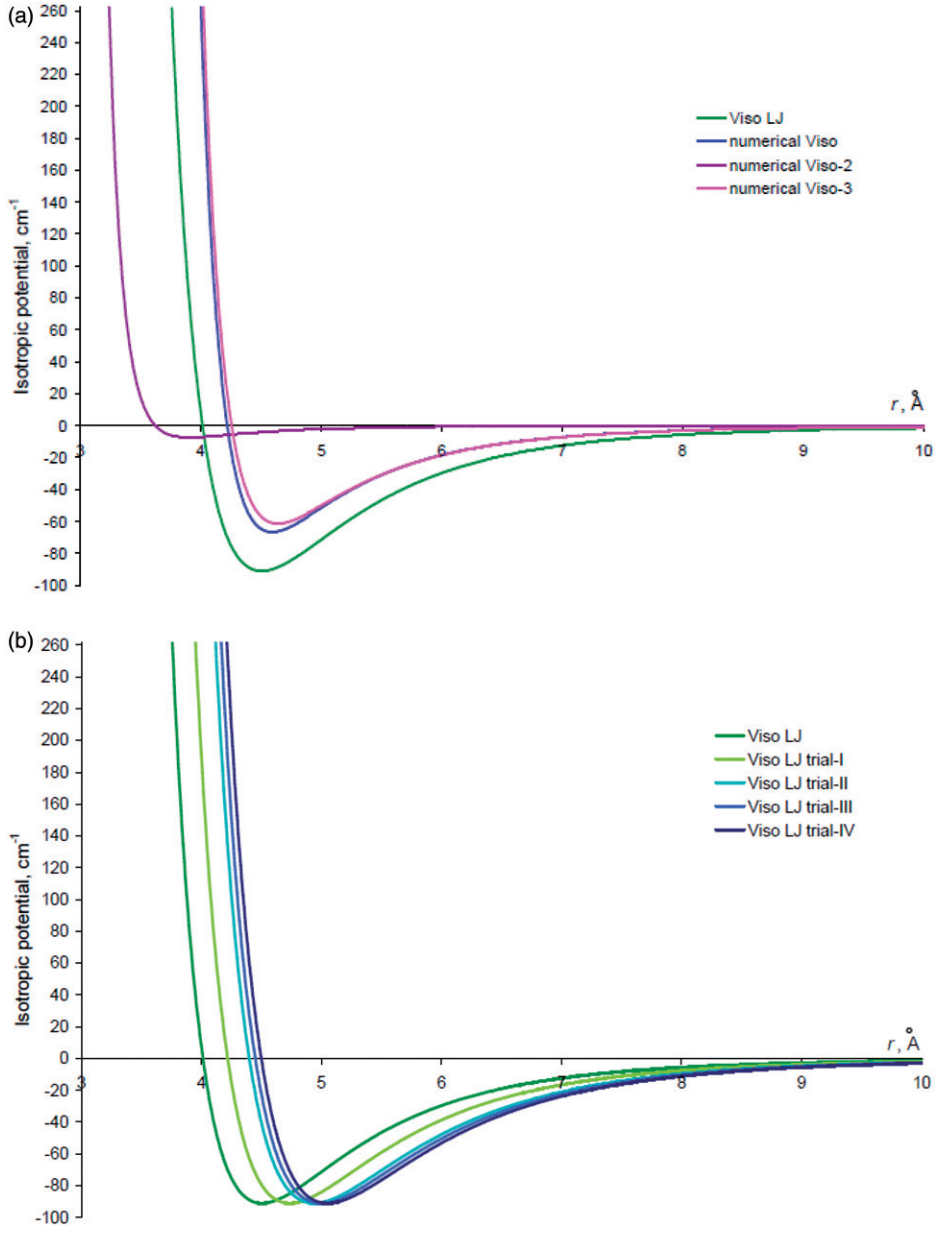

Figure 2. Models of the isotropic potential tested in preliminary computations of line broadening coefficients: with parameterisations available in the literature (a) and with trial parameters of the present work (b).

Downloaded by [University of Lethbridge] at 16:49 28 July 2015

the corresponding room-temperature line widths can be seen in Figure 3(b). As can be stated from this figure, the use of higher σ-values improves the agreement with the measurements for high J, but these σ-values should not be too high in order to not reduce excessively the contributions from the electrostatic interactions for low J-values. The role of the N_2 quadrupole moment is shown for the 'trial-IV' curves: $Q_{N2} = 1.3 \cdot 10^{-26}$ esu cm^2 [8] (curve 'Viso LJ trial-IV'), $Q_{N2} = -1.4 \times 10^{-26}$ esu cm^2 [35] (curve 'Viso LJ trial-IV*') and $Q_{N2} = -1.52 \times 10^{-26}$ esu cm^2 [31] (curve'Viso LJ trial-IV**'). The best agreement between the calculated and experimental broadening coefficients is obtained for the isotropic Lennard–Jones potential with the parameters $\varepsilon = 131.1$ K, $\sigma = 4.45$ Å and the nitrogen quadrupole moment from Ref. [31] (curve 'Viso LJ trial-III**' in Figure 3(b)); this parameterisation of the C_2H_2–N_2 interaction potential has been retained therefore for final calculations of line widths and shifts at various temperatures.

Since the vibrational dependence of neither isotropic nor anisotropic interaction potential of C_2H_2 with

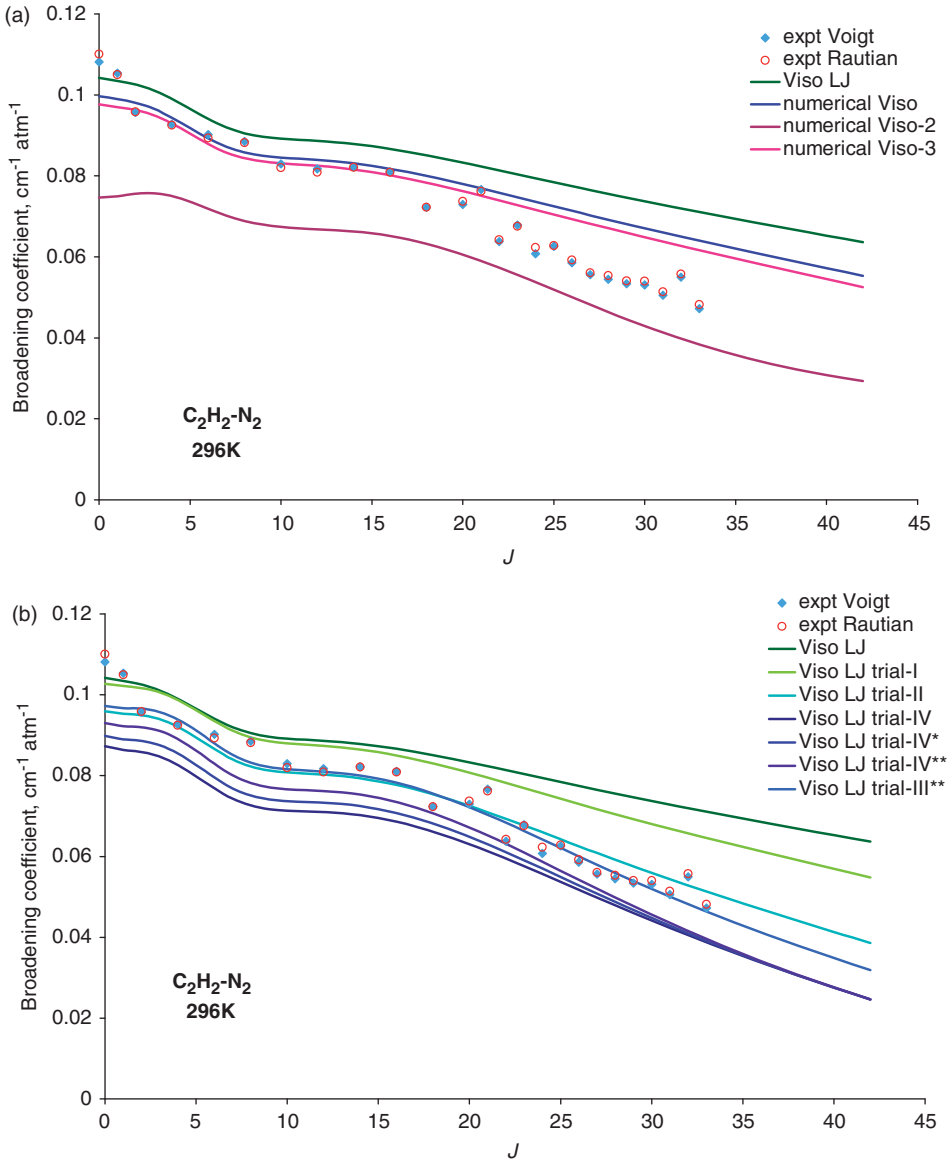

Figure 3. C_2H_2–N_2 line broadening coefficients calculated with the isotropic potentials of Figure 2(a) and (b) at 296 K in comparison with the experimental results of the present work. The curves without asterisk correspond to the quadrupole moment of N_2 equal to -1.3×10^{-26} esu cm^2 [8], the curve marked with an asterisk is obtained with $Q_{N2} = -1.4 \times 10^{-26}$ esu cm^2 [34] and the curves with double asterisks are assimilated with $Q_{N2} = -1.52 \times 10^{-26}$ esu cm^2 [30].

Downloaded by [University of Lethbridge] at 16:49 28 July 2015

Downloaded by [University of Lethbridge] at 16:49 28 July 2015

N_2 is available for any vibrational motion of the active molecule, for the calculation of line shifts we have followed the procedure described in Ref. [36]. First, neglecting Im S_2 in the second exponent of Equation (5), we have computed the contribution coming from the vibrational dephasing S_1 term modelled by

$$S_1 = \frac{3}{2}\frac{\pi\varepsilon\sigma}{\hbar v_c'}\frac{\Delta C_6}{C_6}\left[\frac{21}{32}\left(\frac{\sigma}{r_c}\right)^{11} y - \left(\frac{\sigma}{r_c}\right)^{5}\right] \qquad (12)$$

with $v_c' = \bar{v}\left\{1 + 8\varepsilon/(m^{\circ}\bar{v}^2)[5(\sigma/r_c)^{12} - 2(\sigma/r_c)^6]\right\}^{1/2}$, and adjusted the fitting parameters $\Delta C_6/C_6$ and y on the high-J values of the experimental line-shifting coefficients at 296 K (Figure 4); the best overall agreement has been obtained for $\Delta C_6/C_6 = 0.005$ and $y = 0.7$. Then, the 'rotational' contribution, due to ImS_2 and responsible for the asymmetry of the shift in the R- and P-branches, has been added, leading to slight modifications of the line shifts for low values of the rotational quantum number.

4. Results

The experimental N_2-broadening coefficients retrieved in the present work are given in Table 3(a) for the Voigt model and in Table 3(b) for the hard-collision model. For the room temperature coefficients, their comparison with the results available in the literature from previous studies and with the calculations detailed in Section 3 can be seen in Figure 5 as a function of the quantum number m ($m = -J''$ for the P-branch and $m = J''+1$ for the R-branch). Our measurements show a good agreement with the experimental values of broadening coefficients for other bands, and our theoretical results (see Table 3(c) for their numerical values) compare very favourably with all sets of experimental data.

The N_2-pressure induced shift coefficients for the Voigt and hard-collision profiles are listed in Table 4(a) and (b), respectively; the calculated semi-classical values can be found in Table 4(c). A comparison of our results with those available in the literature for the room-temperature case is given in Figure 6.

The temperature-dependence exponents, n, of N_2-broadening coefficients were calculated using Equation (1) and the N_2-broadening coefficients obtained with both Voigt and hard-collision models. The results are presented in Table 5 and plotted in Figure 7 along with values issued from our calculated N_2-broadening coefficients. For m > 22 the theoretical values are not shown because of insufficient quality of linear regression analysis. Within the considered range of m-values, we notice a good agreement between the theoretical and experimental values of n.

The temperature dependencies of N_2-shift coefficients were retrieved using the linear expression of Equation (3) and the quadratic expression of Equation (4). The results are given in Tables 6 and 7, respectively, together with theoretical values deduced from the semi-classically calculated line shifts. Figure 8(a) presents the results of Table 6 and Figure 8(b) and (c) show those of Table 7. According to the three panels of Figure 8, the quadratic expression

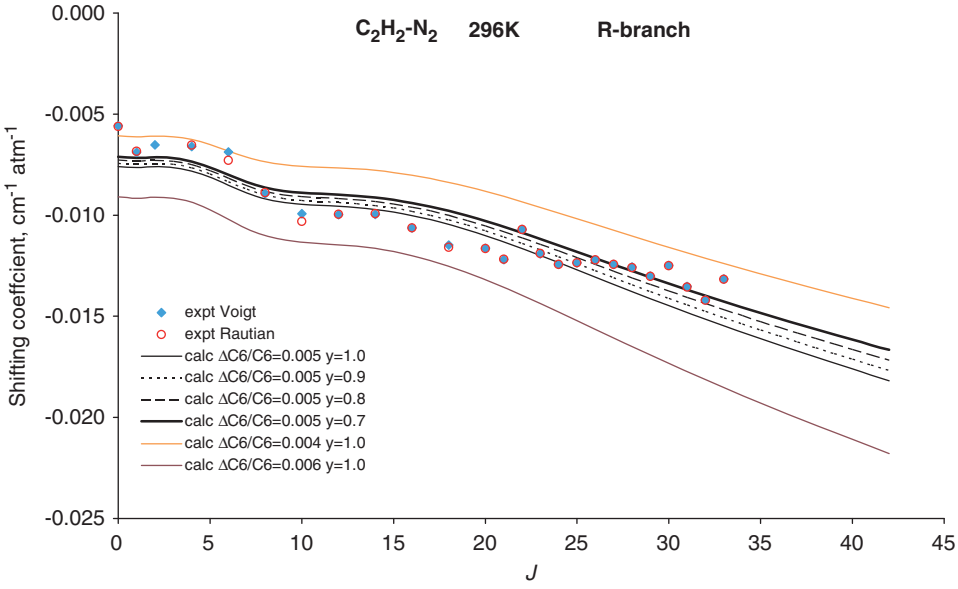

Figure 4. Room-temperature line-shifting coefficients calculated with the vibrational dephasing contribution for various values of fitting parameters accounting for the vibrational dependence of the isotropic potential.

Table 3(a). N_2-broadening coefficients ($cm^{-1}\,atm^{-1}$) retrieved with the Voigt profile.

Lines	*m*	213 K	233 K	253 K	273 K	296 K	313 K	333 K
P(31)	−31	0.0602(6)	0.0551(2)	0.0499(4)	0.0487(4)	0.0448(3)	0.0451(3)	0.0435(3)
P(30)	−30	0.0647(14)	0.0611(7)	0.0589(7)	0.0566(6)	0.0507(5)	0.0524(5)	0.0527(5)
P(29)	−29	0.0725(2)	0.0655(3)	0.0633(4)	0.0611(1)	0.0549(2)	0.0479(2)	0.0586(2)
P(28)	−28	0.0702(7)	0.0650(4)	0.0639(4)	0.0550(5)	0.0521(3)	0.0516(4)	0.0467(4)
P(27)	−27	0.0705(3)	0.0656(4)	0.0639(5)	0.0585(5)	0.0606(3)	0.0537(6)	0.0497(6)
P(26)	−26	0.0747(7)	0.0688(6)	0.0667(6)	0.0625(2)	0.0546(21)	0.0550(6)	0.0544(6)
P(25)	−25	0.0751(1)		0.0662(2)	0.0635(5)	0.0586(3)	0.0570(4)	0.0538(4)
P(24)	−24	0.0808(3)	0.0765(3)	0.0724(4)	0.0678(5)	0.0523(0)	0.0631(1)	0.0610(1)
P(23)	−23	0.0829(3)	0.0784(2)	0.0795(3)	0.0736(1)	0.0584(5)	0.0610(8)	0.0620(8)
P(22)	−22	0.0831(3)	0.0804(3)	0.0786(4)	0.0724(7)	0.0526(2)	0.0730(5)	0.0640(5)
P(21)	−21	0.0871(3)	0.0815(2)	0.0787(4)	0.0747(4)	0.0538(2)	0.0652(4)	0.0595(4)
P(20)	−20	0.0864(3)	0.0822(2)	0.0818(3)	0.0722(1)	0.0547(8)	0.0677(2)	0.0671(2)
P(18)	−18	0.1006(4)	0.0957(3)	0.0885(1)	0.0831(2)	0.0571(7)	0.0662(4)	0.0613(4)
P(16)	−16	0.0905(2)	0.0876(15)	0.0795(5)	0.0754(4)	0.0595(4)	0.0665(4)	0.0600(4)
P(14)	−14	0.0956(5)	0.0962(4)	0.0813(2)	0.0811(2)	0.0652(7)	0.0725(7)	0.0682(7)
P(12)	−12	0.0997(2)	0.0963(4)	0.0855(5)	0.0838(23)	0.0689(2)	0.0747(4)	0.0700(4)
P(10)	−10	0.1074(13)	0.0979(7)	0.0907(7)	0.0851(5)	0.0730(0)	0.0721(5)	0.0708(5)
P(8)	−8	0.1090(6)	0.1011(0)	0.0925(7)	0.0861(2)	0.0802(0)	0.0726(2)	0.0735(2)
P(6)	−6	0.1130(3)	0.1061(7)	0.0986(8)	0.0913(4)	0.0921(0)	0.0828(7)	0.0815(7)
P(4)	−4	0.1332(19)	0.1115(6)	0.1009(5)	0.0995(6)	0.0960(21)	0.0951(6)	0.0889(6)
P(2)	−2	0.1348(5)	0.1269(4)	0.1104(4)	0.1125(2)	0.1022(4)	0.1000(8)	0.0922(8)
P(1)	−1	0.1455(7)	0.1303(1)	0.1208(6)	0.1147(3)	0.1057(19)	0.1044(8)	0.0970(8)
R(0)	1	0.1428(10)	0.1355(10)	0.1210(19)	0.1129(23)	0.1081(7)	0.1065(6)	0.1005(15)
R(1)	2	0.1350(35)	0.1304(17)	0.1147(19)	0.1123(17)	0.1053(13)	0.1071(7)	0.0997(8)
R(2)	4	0.1282(10)	0.1191(4)	0.1103(10)	0.1052(7)	0.0957(9)	0.0925(6)	0.0878(5)
R(4)	6	0.1227(14)	0.1176(12)	0.1058(12)	0.1044(6)	0.0928(6)	0.0914(5)	0.0857(5)
R(6)	8	0.1126(22)	0.1075(11)	0.0972(26)	0.0998(14)	0.0902(7)	0.0829(13)	0.0778(10)
R(8)	10	0.1062(14)	0.1056(12)	0.0905(24)	0.0996(6)	0.0885(3)	0.0835(7)	0.0786(6)
R(10)	12	0.1011(19)	0.0972(24)	0.0898(21)	0.0907(7)	0.0830(2)	0.0797(5)	0.0738(9)
R(12)	14	0.1032(6)	0.1015(7)	0.0893(8)	0.0870(11)	0.0817(8)	0.0823(5)	0.0736(6)
R(14)	16	0.1002(7)	0.0973(6)	0.0868(11)	0.0860(5)	0.0822(4)	0.0820(9)	0.0738(7)
R(16)	18	0.1013(2)	0.0967(3)	0.0896(2)	0.0818(5)	0.0810(3)	0.0778(2)	0.0713(4)
R(18)	20	0.0932(3)	0.0892(3)	0.0872(1)	0.0824(3)	0.0723(5)	0.0724(3)	0.0692(3)
R(20)	21	0.0877(5)	0.0814(3)	0.0805(1)	0.0708(3)	0.0730(3)	0.0708(4)	0.0643(3)
R(21)	22	0.0883(4)	0.0871(3)	0.0839(4)	0.0793(4)	0.0766(4)	0.0707(5)	0.0701(4)
R(22)	23	0.0804(5)	0.0740(3)	0.0707(3)	0.0672(2)	0.0638(3)	0.0626(2)	0.0592(2)
R(23)	24	0.0793(3)	0.0774(3)	0.0742(3)	0.0693(4)	0.0678(3)	0.0648(3)	0.0628(4)
R(24)	25	0.0760(4)	0.0706(5)	0.0691(5)	0.0653(3)	0.0608(3)	0.0600(2)	0.0566(2)
R(25)	26	0.0748(2)	0.0712(1)	0.0674(2)	0.0643(2)	0.0626(1)	0.0606(1)	0.0579(2)
R(26)	27	0.0752(6)	0.0670(5)	0.0633(3)	0.0569(4)	0.0586(2)	0.0556(2)	0.0554(2)
R(27)	28	0.0659(4)	0.0624(3)	0.0598(3)	0.0576(2)	0.0556(4)	0.0549(2)	0.0535(2)
R(28)	29	0.0648(5)	0.0625(3)	0.0601(3)	0.0566(1)	0.0545(2)	0.0529(2)	0.0500(2)
R(29)	30	0.0627(7)	0.0599(5)	0.0571(2)	0.0554(1)	0.0534(1)	0.0513(1)	0.0489(1)
R(30)	31	0.0560(17)	0.0616(11)	0.0570(8)	0.0537(3)	0.0531(5)	0.0483(4)	0.0479(3)
R(31)	32	0.0614(3)	0.0581(3)	0.0522(3)	0.0518(2)	0.0505(2)	0.0472(2)	0.0460(2)
R(32)	33	0.0880(13)	0.0661(13)	0.0595(11)	0.0546(8)	0.0550(7)	0.0513(6)	0.0400(4)
R(33)	34	0.0577(16)	0.0550(8)	0.0494(7)	0.0478(3)	0.0472(3)	0.0442(2)	0.0413(4)

Downloaded by [University of Lethbridge] at 16:49 28 July 2015

Table 3(b). N_2-broadening coefficients ($cm^{-1}\,atm^{-1}$) retrieved with the hard-collision profile.

Lines	*m*	213 K	233 K	253 K	273 K	296 K	313 K	333 K
P(31)	−31	0.0610(8)	0.0554(3)	0.0507(6)	0.0494(5)	0.0416(5)	0.0460(5)	0.0443(4)
P(30)	−30	0.0652(16)	0.0616(10)	0.0595(9)	0.0573(9)	0.0441(6)	0.0532(7)	0.0535(10)
P(29)	−29	0.0728(3)	0.0660(5)	0.0639(5)	0.0614(2)	0.0513(1)	0.0485(2)	0.0586(4)
P(28)	−28	0.0707(11)	0.0657(5)	0.0646(6)	0.0558(8)	0.0541(0)	0.0527(6)	0.0476(9)
P(27)	−27	0.0712(5)	0.0664(5)	0.0645(7)	0.0588(7)	0.0608(1)	0.0542(9)	0.0500(2)
P(26)	−26	0.0751(10)	0.0693(9)	0.0672(9)	0.0633(3)	0.0580(7)	0.0558(9)	0.0551(10)
P(25)	−25	0.0739(3)		0.0666(3)	0.0638(7)	0.0613(1)	0.0571(7)	0.0538(6)
P(24)	−24	0.0812(4)	0.0768(4)	0.0728(6)	0.0683(6)	0.0611(8)	0.0629(1)	0.0616(4)
P(23)	−23	0.0830(5)	0.0785(3)	0.0795(5)	0.0735(1)	0.0627(4)	0.0606(17)	0.0633(10)
P(22)	−22	0.0834(4)	0.0808(4)	0.0790(6)	0.0726(10)	0.0632(3)	0.0734(7)	0.0644(6)
P(21)	−21	0.0871(3)	0.0813(7)	0.0782(8)	0.0741(7)	0.0640(6)	0.0653(5)	0.0583(11)
P(20)	−20	0.0866(4)	0.0824(3)	0.0820(4)	0.0725(1)	0.0687(6)	0.0683(3)	0.0674(9)
P(18)	−18	0.1007(4)	0.0958(4)	0.0885(1)	0.0831(3)	0.0715(0)	0.0663(6)	0.0614(7)
P(16)	−16	0.0902(4)	0.0872(28)	0.0791(9)	0.0750(5)	0.0730(5)	0.0660(8)	0.0595(4)
P(14)	−14	0.0951(14)	0.0958(9)	0.0813(2)	0.0806(3)	0.0749(10)	0.0720(15)	0.0679(4)
P(12)	−12	0.0995(8)	0.0940(13)	0.0855(5)	0.0836(48)	0.0783(14)	0.0742(11)	0.0694(13)
P(10)	−10	0.1074(13)	0.0979(8)	0.0907(8)	0.0851(4)	0.0836(5)	0.0704(10)	0.0694(8)
P(8)	−8	0.1090(6)	0.1008(16)	0.0925(8)	0.0858(4)	0.0893(8)	0.0719(5)	0.0728(9)
P(6)	−6	0.1128(11)	0.1061(9)	0.0985(23)	0.0908(7)	0.0964(7)	0.0824(12)	0.0812(7)
P(4)	−4	0.1324(24)	0.1116(9)	0.1006(11)	0.0994(9)	0.0990(8)	0.0951(10)	0.0890(5)
P(2)	−2	0.1349(8)	0.1270(6)	0.1105(7)	0.1127(2)	0.1071(8)	0.1003(12)	0.0927(6)
P(1)	−1	0.1498(15)	0.1302(12)	0.1207(9)	0.1147(4)	0.1080(14)	0.1044(6)	0.0972(6)
R(0)	1	0.1430(10)	0.1360(10)	0.1214(19)	0.1133(22)	0.1100(7)	0.1068(6)	0.1015(15)
R(1)	2	0.1347(35)	0.1298(17)	0.1141(19)	0.1118(17)	0.1050(13)	0.1069(7)	0.0993(8)
R(2)	4	0.1280(11)	0.1191(4)	0.1103(10)	0.1053(6)	0.0958(9)	0.0929(6)	0.0881(5)
R(4)	6	0.1224(14)	0.1174(12)	0.1054(12)	0.1041(6)	0.0925(7)	0.0914(5)	0.0858(5)
R(6)	8	0.1120(22)	0.1064(11)	0.0967(26)	0.0992(15)	0.0893(15)	0.0829(13)	0.0774(10)
R(8)	10	0.1053(14)	0.1051(12)	0.0898(24)	0.0990(6)	0.0882(3)	0.0828(7)	0.0780(7)
R(10)	12	0.1000(19)	0.0970(24)	0.0890(21)	0.0903(7)	0.0820(5)	0.0797(5)	0.0730(9)
R(12)	14	0.1030(6)	0.1012(7)	0.0889(8)	0.0863(11)	0.0809(8)	0.0819(5)	0.0729(6)
R(14)	16	0.0999(7)	0.0971(6)	0.0863(11)	0.0858(5)	0.0821(4)	0.0817(9)	0.0737(7)
R(16)	18	0.1012(2)	0.0934(3)	0.0895(2)	0.0816(5)	0.0809(3)	0.0778(2)	0.0711(4)
R(18)	20	0.0933(3)	0.0892(3)	0.0873(1)	0.0828(2)	0.0723(5)	0.0725(3)	0.0692(3)
R(20)	21	0.0879(5)	0.0817(3)	0.0807(1)	0.0709(3)	0.0737(3)	0.0687(4)	0.0645(3)
R(21)	22	0.0881(4)	0.0869(3)	0.0836(4)	0.0788(4)	0.0762(4)	0.0692(6)	0.0694(4)
R(22)	23	0.0808(5)	0.0744(3)	0.0711(3)	0.0672(2)	0.0642(3)	0.0628(2)	0.0596(2)
R(23)	24	0.0795(3)	0.0775(3)	0.0741(1)	0.0691(4)	0.0676(3)	0.0644(4)	0.0623(4)
R(24)	25	0.0765(4)	0.0712(5)	0.0696(4)	0.0659(3)	0.0623(1)	0.0606(2)	0.0571(2)
R(25)	26	0.0752(2)	0.0716(1)	0.0678(2)	0.0643(2)	0.0628(1)	0.0608(1)	0.0580(2)
R(26)	27	0.0758(6)	0.0677(5)	0.0641(3)	0.0550(3)	0.0592(2)	0.0565(2)	0.0560(2)
R(27)	28	0.0667(3)	0.0630(3)	0.0604(3)	0.0582(2)	0.0561(4)	0.0554(1)	0.0540(2)
R(28)	29	0.0654(5)	0.0631(3)	0.0609(3)	0.0572(1)	0.0553(2)	0.0537(2)	0.0512(2)
R(29)	30	0.0635(7)	0.0607(5)	0.0580(2)	0.0559(1)	0.0540(1)	0.0521(1)	0.0497(1)
R(30)	31	0.0568(17)	0.0623(11)	0.0579(7)	0.0544(3)	0.0540(5)	0.0494(4)	0.0490(3)
R(31)	32	0.0620(3)	0.0588(3)	0.0529(3)	0.0522(1)	0.0514(2)	0.0480(2)	0.0469(1)
R(32)	33	0.0879(55)	0.0666(13)	0.0604(11)	0.0552(8)	0.0557(7)	0.0520(6)	0.0412(3)
R(33)	34	0.0584(16)	0.0558(8)	0.0504(7)	0.0488(3)	0.0482(3)	0.0452(2)	0.0425(3)

Downloaded by [University of Lethbridge] at 16:49 28 July 2015

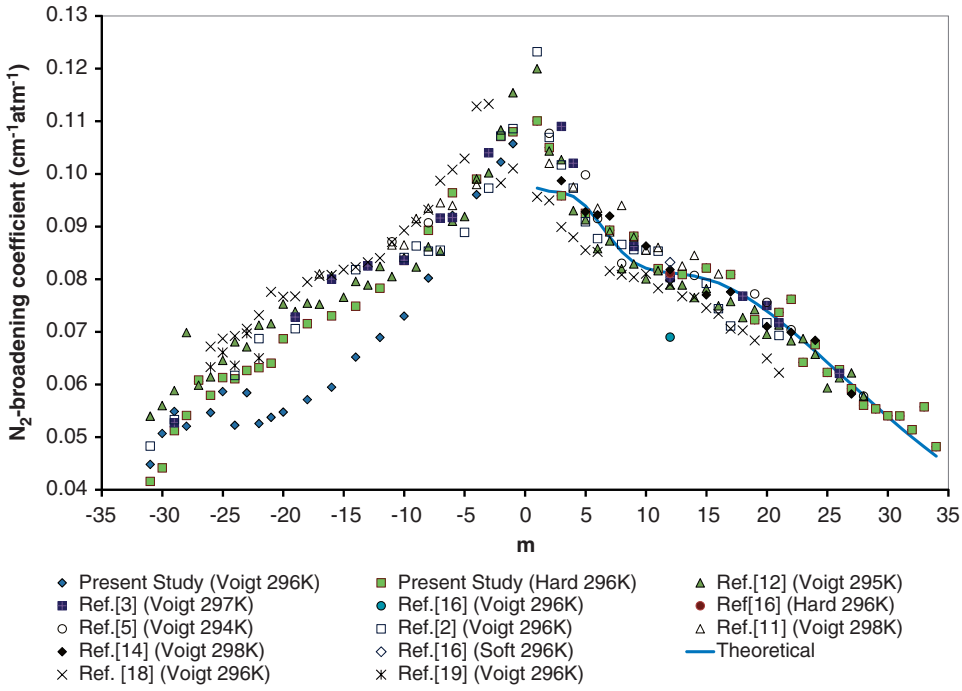

Figure 5. Room temperature N_2-broadening coefficients of C_2H_2 transitions (present sudy and published results) as a function of m, where $m = -J''$ for the P-branch lines and $J''+1$ for the R-branch lines.

Table 3(c). N_2-broadening coefficients ($cm^{-1}\,atm^{-1}$) calculated with the semi-classical approach.

Lines	J	213 K	233 K	253 K	273 K	296 K	313 K	333 K
R(0)	0	0.1296	0.1198	0.1114	0.1042	0.0973	0.0929	0.0879
R(1)	1	0.1285	0.1189	0.1107	0.1035	0.0967	0.0923	0.0873
R(2)	2	0.1277	0.1184	0.1103	0.1033	0.0965	0.0922	0.0873
R(3)	3	0.1254	0.1166	0.1090	0.1022	0.0957	0.0916	0.0868
R(4)	4	0.1218	0.1135	0.1063	0.1000	0.0939	0.0900	0.0855
R(5)	5	0.1173	0.1095	0.1028	0.0968	0.0911	0.0875	0.0833
R(6)	6	0.1131	0.1055	0.0991	0.0934	0.0880	0.0846	0.0806
R(7)	7	0.1101	0.1025	0.0960	0.0905	0.0852	0.0819	0.0781
R(8)	8	0.1085	0.1007	0.0941	0.0885	0.0832	0.0799	0.0761
R(9)	9	0.1079	0.1000	0.0932	0.0875	0.0821	0.0787	0.0748
R(10)	10	0.1076	0.0996	0.0928	0.0870	0.0815	0.0781	0.0741
R(11)	11	0.1072	0.0993	0.0926	0.0867	0.0812	0.0778	0.0738
R(12)	12	0.1064	0.0988	0.0922	0.0864	0.0810	0.0775	0.0736
R(13)	13	0.1052	0.0979	0.0915	0.0859	0.0806	0.0772	0.0733
R(14)	14	0.1036	0.0967	0.0906	0.0852	0.0800	0.0767	0.0729
R(15)	15	0.1015	0.0951	0.0893	0.0842	0.0793	0.0761	0.0724
R(16)	16	0.0990	0.0932	0.0878	0.0829	0.0782	0.0752	0.0717
R(17)	17	0.0962	0.0909	0.0859	0.0814	0.0770	0.0742	0.0708
R(18)	18	0.0932	0.0884	0.0839	0.0797	0.0756	0.0729	0.0697
R(19)	19	0.0899	0.0857	0.0816	0.0778	0.0739	0.0715	0.0685
R(20)	20	0.0865	0.0829	0.0792	0.0757	0.0722	0.0699	0.0671
R(21)	21	0.0831	0.0799	0.0766	0.0735	0.0703	0.0683	0.0657
R(22)	22	0.0796	0.0769	0.0740	0.0712	0.0683	0.0665	0.0641
R(23)	23	0.0760	0.0738	0.0714	0.0689	0.0663	0.0647	0.0625
R(24)	24	0.0726	0.0708	0.0687	0.0665	0.0642	0.0628	0.0608
R(25)	25	0.0692	0.0678	0.0660	0.0641	0.0621	0.0609	0.0591
R(26)	26	0.0659	0.0649	0.0634	0.0618	0.0600	0.0589	0.0573
R(27)	27	0.0628	0.0620	0.0608	0.0595	0.0580	0.0570	0.0556
R(28)	28	0.0597	0.0593	0.0583	0.0572	0.0559	0.0551	0.0539
R(29)	29	0.0567	0.0566	0.0559	0.0550	0.0539	0.0533	0.0522
R(30)	30	0.0539	0.0540	0.0535	0.0528	0.0519	0.0514	0.0505
R(31)	31	0.0512	0.0515	0.0512	0.0507	0.0500	0.0497	0.0488
R(32)	32	0.0485	0.0491	0.0490	0.0486	0.0482	0.0479	0.0472
R(33)	33	0.0460	0.0467	0.0469	0.0467	0.0464	0.0462	0.0456

Downloaded by [University of Lethbridge] at 16:49 28 July 2015

Table 4(a). N_2-shifting coefficients ($cm^{-1}\,atm^{-1}$) retrieved with the Voigt profile.

Lines	*m*	213 K	233 K	253 K	273 K	296 K	313 K	333 K
P(31)	−31	−0.0135(6)	−0.0126(2)	−0.0130(4)	−0.0124(4)	−0.0112(7)	−0.0122(3)	−0.0119(3)
P(30)	−30	−0.0131(10)	−0.0121(7)	−0.0119(7)	−0.0117(6)	−0.0097(18)	−0.0121(5)	−0.0102(7)
P(29)	−29	–0.0134(2)	−0.0134(3)	−0.0136(4)	−0.0126(1)	−0.0120(1)	−0.0096(2)	−0.0124(3)
P(28)	−28	−0.0121(7)	−0.0121(4)	−0.0120(4)	−0.0113(5)	−0.0119(2)	−0.0122(4)	−0.0113(6)
P(27)	−27	−0.0128(3)	−0.0124(4)	−0.0124(5)	−0.0116(5)	−0.0107(2)	−0.0117(6)	−0.0107(2)
P(26)	−26	−0.0126(7)	−0.0124(6)	−0.0119(6)	−0.0118(3)	−0.0102(7)	−0.0116(6)	−0.0109(7)
P(25)	−25	−0.0128(2)		−0.0118(2)	−0.0116(5)	−0.0113(1)	−0.0113(4)	−0.0108(4)
P(24)	−24	−0.0120(3)	−0.0122(3)	−0.0115(4)	−0.0120(5)	−0.0096(36)	−0.0100(0)	−0.0107(3)
P(23)	−23	−0.0125(3)	−0.0123(2)	−0.0117(3)	−0.0114(1)	−0.0100(4)	−0.0109(8)	−0.0103(5)
P(22)	−22	−0.0121(3)	−0.0118(3)	−0.0117(4)	−0.0112(7)	−0.0096(0)	−0.0111(5)	−0.0102(4)
P(21)	−21	−0.0125(2)	−0.0123(3)	−0.0113(4)	−0.0106(4)	−0.0122(2)	−0.0108(4)	−0.0100(4)
P(20)	−20	−0.0114(3)	−0.0113(2)	−0.0107(3)	−0.0109(1)	−0.0104(4)	−0.0114(2)	−0.0100(6)
P(18)	−18	−0.0116(4)	−0.0117(3)	−0.0117(1)	−0.0119(2)	−0.0120(0)	−0.0124(4)	−0.0124(5)
P(16)	−16	−0.0136(2)	−0.0114(15)	−0.0108(5)	−0.0121(4)	−0.0098(2)	−0.0102(4)	−0.0095(2)
P(14)	−14	−0.0118(5)	−0.0102(4)	−0.0100(2)	−0.0119(2)	−0.0094(4)	−0.0092(7)	−0.0083(2)
P(12)	−12	−0.0114(2)	−0.0110(4)	−0.0102(5)	−0.0114(23)	−0.0107(0)	−0.0090(4)	−0.0084(6)
P(10)	−10	−0.0112(13)	−0.0105(7)	−0.0093(8)	−0.0110(5)	−0.0091(0)	−0.0088(5)	−0.0081(4)
P(8)	−8	−0.0110(6)		−0.0089(7)	−0.0105(2)	−0.0099(0)	−0.0076(2)	−0.0071(5)
P(6)	−6	−0.0083(3)	−0.0072(8)	−0.0080(8)	−0.0161(4)	−0.0068(6)	−0.0073(7)	−0.0066(4)
P(4)	−4	−0.0082(19)	−0.0081(6)	−0.0081(5)	−0.0079(6)	−0.0065(7)	−0.0065(6)	−0.0070(3)
P(2)	−2	−0.0076(5)	−0.0076(4)	−0.0072(4)	−0.0074(2)	−0.0050(4)	−0.0055(8)	−0.0063(4)
P(1)	−1	−0.0074(7)	−0.0076(7)	−0.0074(6)	−0.0073(3)	−0.0019(17)	−0.0066(8)	−0.0064(5)
R(0)	1	−0.0051(7)	−0.0045(7)	−0.0039(13)	−0.0012(15)	−0.0056(7)	−0.0037(4)	−0.0041(0)
R(1)	2	−0.0067(5)	−0.0063(5)	−0.0035(6)	−0.0059(6)	−0.0068(7)	−0.0063(3)	−0.0053(4)
R(2)	4	−0.0069(2)	−0.0067(2)	−0.0057(5)	−0.0067(3)		−0.0059(4)	−0.0060(4)
R(4)	6	−0.0049(5)	−0.0068(5)	−0.0057(5)	−0.0079(3)	−0.0065(4)	−0.0060(3)	−0.0055(3)
R(6)	8	−0.0055(4)	−0.0073(4)	−0.0061(8)	−0.0064(6)	−0.0073(9)	−0.0063(6)	−0.0060(5)
R(8)	10	−0.0079(4)	−0.0075(4)	−0.0073(8)	−0.0088(3)	−0.0089(2)	−0.0070(3)	−0.0064(3)
R(10)	12	−0.0090(6)	−0.0080(6)	−0.0074(6)	−0.0100(2)	−0.0103(2)	−0.0077(2)	−0.0075(3)
R(12)	14	−0.0111(2)	−0.0098(3)	−0.0095(2)	−0.0103(4)	−0.0100(4)	−0.0086(2)	−0.0081(3)
R(14)	16	−0.0111(3)	−0.0123(3)	−0.0099(4)	−0.0108(2)	−0.0099(2)	−0.0092(4)	−0.0089(3)
R(16)	18	−0.0137(2)	−0.0131(2)	−0.0120(1)	−0.0115(2)	−0.0106(2)	−0.0098(1)	−0.0094(2)
R(18)	20	−0.0149(2)	−0.0137(2)	−0.0123(0)	−0.0116(1)	−0.0116(4)	−0.0105(2)	−0.0097(2)
R(20)	21	−0.0151(2)	−0.0139(2)	−0.0126(1)	−0.0118(2)	−0.0117(2)	−0.0098(3)	−0.0098(2)
R(21)	22	−0.0152(2)	−0.0143(2)	−0.0135(3)	−0.0123(3)	−0.0122(3)	−0.0112(3)	−0.0103(3)
R(22)	23	−0.0163(2)	−0.0147(2)	−0.0140(2)	−0.0128(1)	−0.0107(3)	−0.0119(1)	−0.0109(2)
R(23)	24	−0.0163(2)	−0.0152(2)	−0.0140(2)	−0.0129(2)	−0.0119(2)	−0.0121(2)	−0.0111(2)
R(24)	25	−0.0162(3)	−0.0147(3)	−0.0146(3)	−0.0133(2)	−0.0124(1)	−0.0117(2)	−0.0105(2)
R(25)	26	−0.0168(1)	−0.0154(1)	−0.0151(1)	−0.0134(1)	−0.0124(1)	−0.0112(1)	−0.0105(1)
R(26)	27	−0.0176(2)	−0.0160(3)	−0.0157(2)	−0.0138(3)	−0.0122(2)	−0.0121(1)	−0.0115(1)
R(27)	28	−0.0174(2)	−0.0160(2)	−0.0156(2)	−0.0140(2)	−0.0124(3)	−0.0124(1)	−0.0118(1)
R(28)	29	−0.0176(2)	−0.0162(2)	−0.0162(2)	−0.0144(1)	−0.0126(2)	−0.0122(1)	−0.0114(1)
R(29)	30	−0.0177(3)	−0.0164(3)	−0.0164(1)	−0.0142(1)	−0.0130(1)	−0.0134(1)	−0.0128(1)
R(30)	31	−0.0174(7)	−0.0164(7)	−0.0159(5)	−0.0141(2)	−0.0125(3)	−0.0123(2)	−0.0122(2)
R(31)	32	−0.0176(2)	−0.0162(2)	−0.0163(2)	−0.0144(1)	−0.0136(2)	−0.0131(1)	−0.0123(1)
R(32)	33	−0.0140(9)	−0.0141(9)	−0.0156(8)	−0.0136(4)	−0.0142(6)	−0.0118(3)	−0.0118(2)
R(33)	34	−0.0175(6)	−0.0167(6)	−0.0167(4)	−0.0151(2)	−0.0132(2)	−0.0133(2)	−0.0125(2)

gives a better agreement between experimental and theoretical temperature dependencies of N_2-shift coefficients.

5. Conclusions

In the present work we have recorded and analyzed the spectral profiles of 47*P*- and *R*-branch lines of C_2H_2 broadened by N_2 over a range of temperatures between 213 and 333 K. A multispectrum fit technique has been used to extract the collisional line shape parameters. N_2-broadening and shift coefficients have been deduced with the Voigt and hard-collision profile models. Using the results obtained for different temperatures and the standard empirical expressions to model the temperature dependence of broadening and shifting coefficients, we have also determined the

Downloaded by [University of Lethbridge] at 16:49 28 July 2015

Table 4(b). N_2-shifting coefficients (cm^{-1} atm^{-1}) retrieved with the hard-collision profile.

Lines	*m*	213 K	233 K	253 K	273 K	296 K	313 K	333 K
P(31)	−31	−0.0135(6)	−0.0126(2)	−0.0130(4)	−0.0124(4)	−0.0112(7)	−0.0122(3)	−0.0119(3)
P(30)	−30	−0.0131(10)	−0.0121(7)	−0.0119(7)	−0.0117(6)	−0.0097(18)	−0.0121(5)	−0.0102(7)
P(29)	−29	−0.0134(2)	−0.0134(3)	−0.0136(4)	−0.0126(1)	−0.0120(1)	−0.0096(2)	−0.0124(3)
P(28)	−28	−0.0121(7)	−0.0121(4)	−0.0120(4)	−0.0113(5)	−0.0119(2)	−0.0122(4)	−0.0113(6)
P(27)	−27	−0.0128(3)	−0.0124(4)	−0.0124(5)	−0.0116(5)	−0.0107(2)	−0.0117(6)	−0.0107(2)
P(26)	−26	−0.0126(7)	−0.0124(6)	−0.0119(6)	−0.0118(3)	−0.0102(7)	−0.0116(6)	−0.0109(7)
P(25)	−25	−0.0128(2)		−0.0118(2)	−0.0116(5)	−0.0113(1)	−0.0113(4)	−0.0108(4)
P(24)	−24	−0.0120(3)	−0.0122(3)	−0.0115(4)	−0.0120(5)	−0.0096(36)	−0.0100(0)	−0.0107(3)
P(23)	−23	−0.0125(3)	−0.0123(2)	−0.0117(3)	−0.0114(1)	−0.0100(4)	−0.0109(8)	−0.0103(5)
P(22)	−22	−0.0121(3)	−0.0118(3)	−0.0117(4)	−0.0112(7)	−0.0096(0)	−0.0111(5)	−0.0102(4)
P(21)	−21	−0.0125(2)	−0.0123(3)	−0.0113(4)	−0.0106(4)	−0.0122(2)	−0.0108(4)	−0.0100(4)
P(20)	−20	−0.0114(3)	−0.0113(2)	−0.0107(3)	−0.0109(1)	−0.0104(4)	−0.0114(2)	−0.0100(6)
P(18)	−18	−0.0116(4)	−0.0117(3)	−0.0117(1)	−0.0119(2)	−0.0120(0)	−0.0124(4)	−0.0124(5)
P(16)	−16	−0.0136(2)	−0.0114(15)	−0.0108(5)	−0.0121(4)	−0.0098(2)	−0.0102(4)	−0.0095(2)
P(14)	−14	−0.0118(5)	−0.0102(4)	−0.0100(2)	−0.0119(2)	−0.0094(4)	−0.0092(7)	−0.0083(2)
P(12)	−12	−0.0114(2)	−0.0110(4)	−0.0102(5)	−0.0114(23)	−0.0107(0)	−0.0090(4)	−0.0084(6)
P(10)	−10	−0.0112(13)	−0.0105(7)	−0.0093(8)	−0.0110(5)	−0.0091(0)	−0.0088(5)	−0.0081(4)
P(8)	−8	−0.0110(6)		−0.0089(7)	−0.0105(2)	−0.0099(0)	−0.0076(2)	−0.0071(5)
P(6)	−6	−0.0083(3)	−0.0072(8)	−0.0080(8)	−0.0161(4)	−0.0068(6)	−0.0073(7)	−0.0066(4)
P(4)	−4	−0.0082(19)	−0.0081(6)	−0.0081(5)	−0.0079(6)	−0.0065(7)	−0.0065(6)	−0.0070(3)
P(2)	−2	−0.0076(5)	−0.0076(4)	−0.0072(4)	−0.0074(2)	−0.0050(4)	−0.0055(8)	−0.0063(4)
P(1)	−1	−0.0074(7)	−0.0076(7)	−0.0074(6)	−0.0073(3)	−0.0019(17)	−0.0066(8)	−0.0064(5)
R(0)	1	−0.0051(7)	−0.0045(7)	−0.0039(13)	−0.0012(15)	−0.0056(7)	−0.0037(4)	−0.0041(0)
R(1)	2	−0.0067(5)	−0.0063(5)	−0.0035(6)	−0.0059(6)	−0.0068(7)	−0.0063(3)	−0.0053(4)
R(2)	4	−0.0069(2)	−0.0067(2)	−0.0057(5)	−0.0067(3)		−0.0059(4)	−0.0060(4)
R(4)	6	−0.0049(5)	−0.0068(5)	−0.0057(5)	−0.0079(3)	−0.0065(4)	−0.0060(3)	−0.0055(3)
R(6)	8	−0.0055(4)	−0.0073(4)	−0.0061(8)	−0.0064(6)	−0.0073(9)	−0.0063(6)	−0.0060(5)
R(8)	10	−0.0079(4)	−0.0075(4)	−0.0073(8)	−0.0088(3)	−0.0089(2)	−0.0070(3)	−0.0064(3)
R(10)	12	−0.0090(6)	−0.0080(6)	−0.0074(6)	−0.0100(2)	−0.0103(2)	−0.0077(2)	−0.0075(3)
R(12)	14	−0.0111(2)	−0.0098(3)	−0.0095(2)	−0.0103(4)	−0.0100(4)	−0.0086(2)	−0.0081(3)
R(14)	16	−0.0111(3)	−0.0123(3)	−0.0099(4)	−0.0108(2)	−0.0099(2)	−0.0092(4)	−0.0089(3)
R(16)	18	−0.0137(2)	−0.0131(2)	−0.0120(1)	−0.0115(2)	−0.0106(2)	−0.0098(1)	−0.0094(2)
R(18)	20	−0.0149(2)	−0.0137(2)	−0.0123(0)	−0.0116(1)	−0.0116(4)	−0.0105(2)	−0.0097(2)
R(20)	21	−0.0151(2)	−0.0139(2)	−0.0126(1)	−0.0118(2)	−0.0117(2)	−0.0098(3)	−0.0098(2)
R(21)	22	−0.0152(2)	−0.0143(2)	−0.0135(3)	−0.0123(3)	−0.0122(3)	−0.0112(3)	−0.0103(3)
R(22)	23	−0.0163(2)	−0.0147(2)	−0.0140(2)	−0.0128(1)	−0.0107(3)	−0.0119(1)	−0.0109(2)
R(23)	24	−0.0163(2)	−0.0152(2)	−0.0140(2)	−0.0129(2)	−0.0119(2)	−0.0121(2)	−0.0111(2)
R(24)	25	−0.0162(3)	−0.0147(3)	−0.0146(3)	−0.0133(2)	−0.0124(1)	−0.0117(2)	−0.0105(2)
R(25)	26	−0.0168(1)	−0.0154(1)	−0.0151(1)	−0.0134(1)	−0.0124(1)	−0.0112(1)	−0.0105(1)
R(26)	27	−0.0176(2)	−0.0160(3)	−0.0157(2)	−0.0138(3)	−0.0122(2)	−0.0121(1)	−0.0115(1)
R(27)	28	−0.0174(2)	−0.0160(2)	−0.0156(2)	−0.0140(2)	−0.0124(3)	−0.0124(1)	−0.0118(1)
R(28)	29	−0.0176(2)	−0.0162(2)	−0.0162(2)	−0.0144(1)	−0.0126(2)	−0.0122(1)	−0.0114(1)
R(29)	30	−0.0177(3)	−0.0164(3)	−0.0164(1)	−0.0142(1)	−0.0130(1)	−0.0134(1)	−0.0128(1)
R(30)	31	−0.0174(7)	−0.0164(7)	−0.0159(5)	−0.0141(2)	−0.0125(3)	−0.0123(2)	−0.0122(2)
R(31)	32	−0.0176(2)	−0.0162(2)	−0.0163(2)	−0.0144(1)	−0.0136(2)	−0.0131(1)	−0.0123(1)
R(32)	33	−0.0140(9)	−0.0141(9)	−0.0156(8)	−0.0136(4)	−0.0142(6)	−0.0118(3)	−0.0118(2)
R(33)	34	−0.0175(6)	−0.0167(6)	−0.0167(4)	−0.0151(2)	−0.0132(2)	−0.0133(2)	−0.0125(2)

Downloaded by [University of Lethbridge] at 16:49 28 July 2015

Table 4(c). N_2-shifting coefficients ($cm^{-1}\,atm^{-1}$) calculated with the semi-classical approach.

Lines	*J*	213 K	233 K	253 K	273 K	296 K	313 K	333 K
R(0)	0	−0.0094	−0.0089	−0.0084	−0.0080	−0.0066	−0.0073	−0.0069
R(1)	1	−0.0093	−0.0088	−0.0084	−0.0079	−0.0068	−0.0072	−0.0068
R(2)	2	−0.0093	−0.0088	−0.0084	−0.0080	−0.0067	−0.0072	−0.0069
R(3)	3	−0.0088	−0.0083	−0.0079	−0.0077	−0.0070	−0.0071	−0.0068
R(4)	4	−0.0082	−0.0080	−0.0076	−0.0073	−0.0078	−0.0066	−0.0064
R(5)	5	−0.0090	−0.0083	−0.0077	−0.0073	−0.0083	−0.0067	−0.0064
R(6)	6	−0.0099	−0.0090	−0.0084	−0.0080	−0.0085	−0.0071	−0.0067
R(7)	7	−0.0105	−0.0099	−0.0092	−0.0085	−0.0089	−0.0074	−0.0071
R(8)	8	−0.0111	−0.0103	−0.0097	−0.0091	−0.0088	−0.0080	−0.0075
R(9)	9	−0.0116	−0.0105	−0.0098	−0.0093	−0.0090	−0.0082	−0.0078
R(10)	10	−0.0120	−0.0111	−0.0102	−0.0094	−0.0091	−0.0083	−0.0080
R(11)	11	−0.0118	−0.0111	−0.0104	−0.0097	−0.0089	−0.0085	−0.0080
R(12)	12	−0.0118	−0.0109	−0.0103	−0.0098	−0.0090	−0.0087	−0.0082
R(13)	13	−0.0120	−0.0111	−0.0103	−0.0097	−0.0090	−0.0086	−0.0082
R(14)	14	−0.0122	−0.0113	−0.0105	−0.0098	−0.0091	−0.0087	−0.0082
R(15)	15	−0.0126	−0.0115	−0.0107	−0.0099	−0.0092	−0.0088	−0.0083
R(16)	16	−0.0129	−0.0118	−0.0109	−0.0101	−0.0094	−0.0089	−0.0084
R(17)	17	−0.0134	−0.0122	−0.0112	−0.0104	−0.0096	−0.0091	−0.0085
R(18)	18	−0.0139	−0.0126	−0.0115	−0.0106	−0.0098	−0.0092	−0.0087
R(19)	19	−0.0144	−0.0130	−0.0119	−0.0109	−0.0100	−0.0095	−0.0089
R(20)	20	−0.0149	−0.0135	−0.0122	−0.0112	−0.0103	−0.0097	−0.0091
R(21)	21	−0.0155	−0.0139	−0.0126	−0.0116	−0.0106	−0.0099	−0.0093
R(22)	22	−0.0161	−0.0144	−0.0130	−0.0119	−0.0109	−0.0102	−0.0095
R(23)	23	−0.0166	−0.0149	−0.0135	−0.0123	−0.0112	−0.0105	−0.0098
R(24)	24	−0.0172	−0.0154	−0.0139	−0.0127	−0.0115	−0.0108	−0.0100
R(25)	25	−0.0178	−0.0159	−0.0143	−0.0130	−0.0118	−0.0110	−0.0103
R(26)	26	−0.0183	−0.0163	−0.0147	−0.0134	−0.0121	−0.0113	−0.0105
R(27)	27	−0.0188	−0.0168	−0.0151	−0.0138	−0.0124	−0.0116	−0.0108
R(28)	28	−0.0193	−0.0173	−0.0155	−0.0141	−0.0128	−0.0119	−0.0110
R(29)	29	−0.0198	−0.0177	−0.0159	−0.0145	−0.0131	−0.0122	−0.0113
R(30)	30	−0.0203	−0.0181	−0.0163	−0.0148	−0.0134	−0.0125	−0.0116
R(31)	31	−0.0208	−0.0185	−0.0167	−0.0152	−0.0137	−0.0128	−0.0118
R(32)	32	−0.0212	−0.0189	−0.0171	−0.0155	−0.0140	−0.0130	−0.0121
R(33)	33	−0.0217	−0.0193	−0.0174	−0.0158	−0.0143	−0.0133	−0.0123

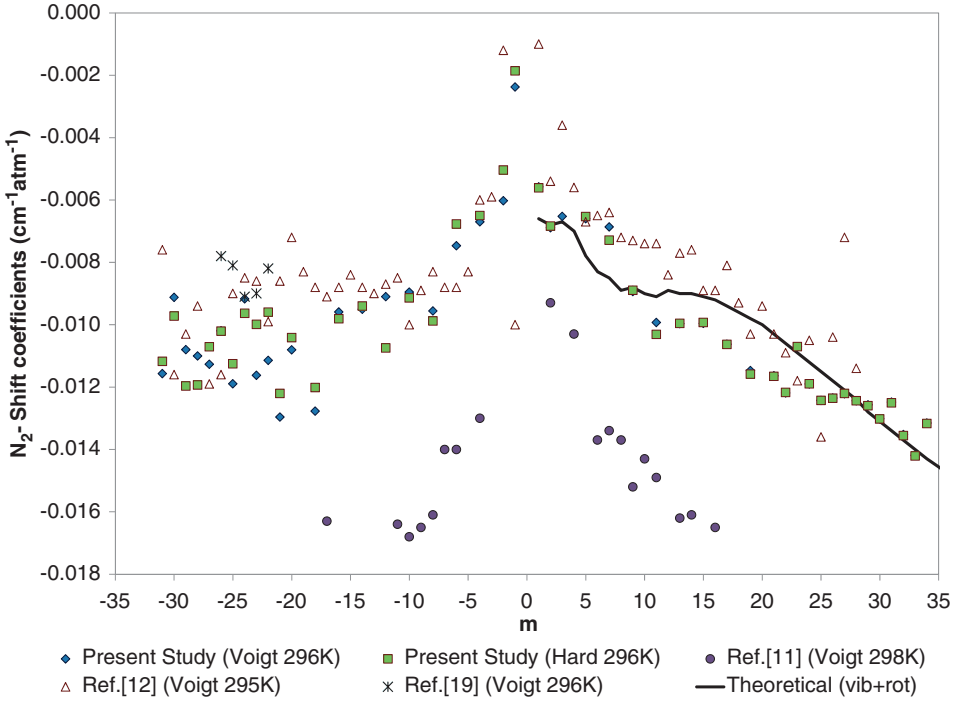

Figure 6. Overlaid experimental, theoretical and published room temperature N_2-shift coefficients of C_2H_2 transitions.

Downloaded by [University of Lethbridge] at 16:49 28 July 2015

Table 5. N_2-broadening coefficients $\gamma^0_{N2}(cm^{-1}\,atm^{-1})$ at 296 K and their temperature dependence exponents n. The experimental results are derived from measurements assuming the Voigt and hard-collision lineshapes (values quoted in parentheses correspond to one standard deviation). The theoretical values are calculated for the R-branch only (P- and R-branches are nearly symmetric when put in function of m); the theoretical temperature exponents for $m > 22$ are not shown because of insufficient quality of linear regression.

Line	m	$\gamma^0_{N2\ Voigt}(296)$	$\gamma^0_{N2\ Hard}(296)$	$\gamma^0_{N2\ calc}(296)$	n_{Voigt}	n_{hard}	n_{calc}
P(31)	−31	0.0448(3)	0.0416(4)	–	0.6140(3)	0.5820(3)	–
P(30)	−30	0.0507(5)	0.0441(4)	–	0.6133(3)	0.6412(3)	–
P(29)	−29	0.0549(2)	0.0513(5)	–	0.6870(3)	0.6673(3)	–
P(28)	−28	0.0521(3)	0.0541(5)	–	0.8166(4)	0.7446(4)	–
P(27)	−27	0.0606(3)	0.0608(6)	–	0.7070(4)	0.7195(4)	–
P(26)	−26	0.0546(21)	0.0580(6)	–	0.7714(4)	0.7261(4)	–
P(25)	−25	0.0586(3)	0.0613(6)	–	0.7415(4)	0.6910(3)	–
P(24)	−24	0.0523(0)	0.0611(6)	–	0.7662(4)	0.6815(3)	–
P(23)	−23	0.0584(5)	0.0627(6)	–	0.8113(4)	0.7530(4)	–
P(22)	−22	0.0526(2)	0.0632(6)	–	0.7652(4)	0.7546(4)	–
P(21)	−21	0.0538(2)	0.0640(6)	–	0.8265(4)	0.8165(4)	–
P(20)	−20	0.0547(8)	0.0687(7)	–	0.8263(4)	0.7442(4)	–
P(18)	−18	0.0571(7)	0.0715(7)	–	0.8904(4)	0.7902(4)	–
P(16)	−16	0.0595(4)	0.0730(7)	–	0.8878(4)	0.7834(4)	–
P(14)	−14	0.0652(7)	0.0749(7)	–	0.8769(4)	0.7964(4)	–
P(12)	−12	0.0689(2)	0.0783(8)	–	0.8860(4)	0.7837(4)	–
P(10)	−10	0.0730(0)	0.0836(8)	–	0.8663(4)	0.7884(4)	–
P(8)	−8	0.0802(0)	0.0893(9)	–	0.8900(4)	0.8220(4)	–
P(6)	−6	0.0921(0)	0.0964(10)	–	0.7646(4)	0.7262(4)	–
P(4)	−4	0.0960(21)	0.0990(10)	–	0.8179(4)	0.7427(4)	–
P(2)	−2	0.1022(4)	0.1071(11)	–	0.8116(4)	0.7765(4)	–
P(1)	−1	0.1057(19)	0.1080(11)	–	0.8648(4)	0.8476(4)	–
R(0)	1	0.1081(7)	0.1100(11)	0.0973	0.7947(4)	0.7755(4)	0.8673
R(1)	2	0.1053(13)	0.1050(10)	0.0967	0.7145(4)	0.7155(4)	0.8631
R(2)	3	0.0957(9)	0.0958(10)	0.0965	0.8547(4)	0.8438(4)	0.8487
R(4)	5	0.0928(6)	0.0925(9)	0.0939	0.8204(4)	0.8137(4)	0.7905
R(6)	7	0.0902(7)	0.0893(9)	0.0880	0.8070(4)	0.7997(4)	0.7553
R(8)	9	0.0885(3)	0.0882(9)	0.0832	0.6955(3)	0.6590(3)	0.7925
R(10)	11	0.0830(2)	0.0820(8)	0.0815	0.6751(3)	0.6745(3)	0.8315
R(12)	13	0.0817(8)	0.0809(8)	0.0810	0.7290(4)	0.7447(4)	0.8248
R(14)	15	0.0822(4)	0.0821(8)	0.0800	0.6909(3)	0.6645(3)	0.7847
R(16)	17	0.0810(3)	0.0809(8)	0.0782	0.7575(4)	0.7294(4)	0.7238
R(18)	19	0.0723(5)	0.0723(7)	0.0756	0.7150(4)	0.7166(4)	0.6511
R(20)	21	0.0730(3)	0.0737(7)	0.0722	0.6240(3)	0.6503(3)	0.5703
R(21)	22	0.0766(4)	0.0762(8)	0.0703	0.5662(3)	0.5984(3)	0.5282
R(22)	23	0.0638(3)	0.0642(6)	0.0683	0.6521(3)	0.6512(3)	–
R(23)	24	0.0678(3)	0.0676(7)	0.0663	0.5457(3)	0.5698(3)	–
R(24)	25	0.0608(3)	0.0623(6)	0.0642	0.6400(3)	0.6234(3)	–
R(25)	26	0.0626(1)	0.0628(6)	0.0621	0.5578(3)	0.5653(3)	–
R(26)	27	0.0586(2)	0.0592(6)	0.0600	0.6672(3)	0.6593(3)	–
R(27)	28	0.0556(4)	0.0561(6)	0.0580	0.5713(3)	0.5713(3)	–
R(28)	29	0.0545(2)	0.0553(6)	0.0559	0.6008(3)	0.5490(3)	–
R(29)	30	0.0534(1)	0.0540(5)	0.0539	0.5354(3)	0.5316(3)	–
R(30)	31	0.0531(5)	0.0540(5)	0.0519	0.5323(3)	0.5323(3)	–
R(31)	32	0.0505(2)	0.0514(5)	0.0500	0.5622(3)	0.5748(3)	–
R(32)	33	0.0550(7)	0.0557(6)	0.0482			–
R(33)	34	0.0472(3)	0.0482(5)	0.0464	0.6035(3)	0.6197(3)	–

Downloaded by [University of Lethbridge] at 16:49 28 July 2015

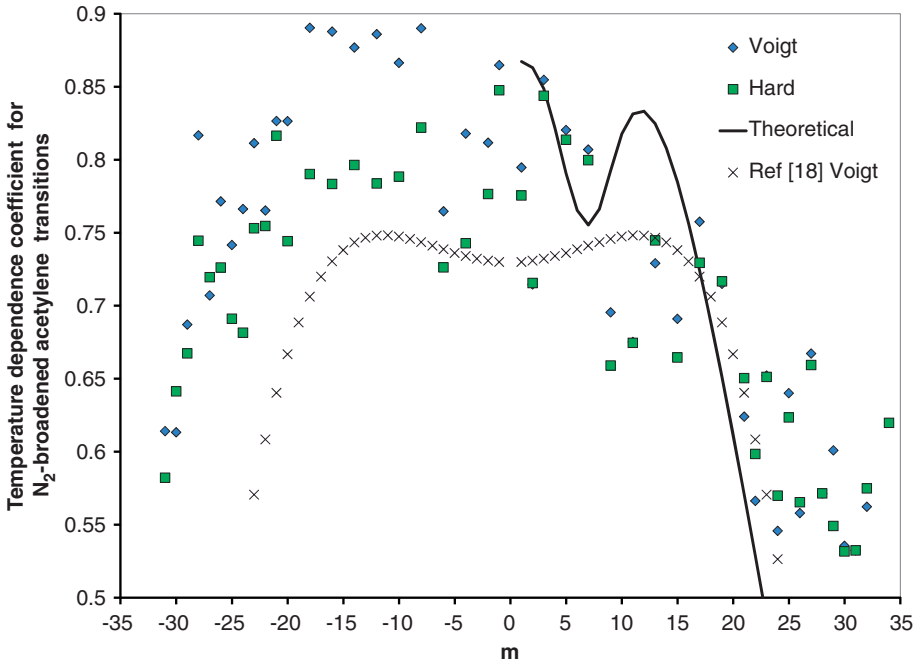

Figure 7. Theoretical and experimental temperature-dependence exponents, n, for the N_2-broadening coefficients of C_2H_2 transitions obtained from Equation (1).

Table 6. N_2-shifting coefficients $\delta^0_{N_2}$ ($cm^{-1}\,atm^{-1}$) at 296 K and their temperature dependence coefficients δ'_{N_2} (according to Equation 3). The experimental results are derived from measurements assuming the Voigt and hard-collision lineshapes (values quoted in parentheses correspond to one standard deviation). The theoretical values are calculated for the *R*-branch only (except very low *m*-values, shifts in the *P*- and *R*-branches are symmetric).

Line	m	$\delta^0_{N2\ Voigt}(296)$	$\delta^0_{N2\ hard}(296)$	$\delta^0_{calc}(296)$	$\delta'_{Voigt} \times 105$	$\delta'_{hard} \times 105$	$\delta'_{calc} \times 105$
P(31)	−31	−0.0122(5)	−0.0120(5)	–	1.3(1)	0.8(1)	–
P(30)	−30	−0.0110(5)	−0.0112(5)	–	0.8(1)	0.9(1)	–
P(29)	−29	−0.0122(5)	−0.0124(6)	–	1.3(1)	0.9(1)	–
P(28)	−28	−0.0111(5)	−0.0119(5)	–	0.9(1)	0.1(0)	–
P(27)	−27	−0.0116(5)	−0.0114(5)	–	1.1(1)	1.0(1)	–
P(26)	−26	−0.0113(5)	−0.0117(5)	–	1.1(1)	1.0(1)	–
P(25)	−25	−0.0114(5)	−0.0113(5)	–	1.1(1)	1.1(1)	–
P(24)	−24	−0.0109(5)	−0.0108(5)	–	1.3(1)	1.5(2)	–
P(23)	−23	−0.0113(5)	−0.0107(5)	–	1.4(1)	1.3(1)	–
P(22)	−22	−0.0116(5)	−0.0107(5)	–	1.1(1)	1.6(2)	–
P(21)	−21	−0.0114(5)	−0.0110(5)	–	1.0(1)	1.7(2)	–
P(20)	−20	−0.0105(5)	−0.0107(5)	–	1.2(1)	0.8(1)	–
P(18)	−18	−0.0127(6)	−0.0121(5)	–	1.3(1)	−0.7(0)	–
P(16)	−16	−0.0103(5)	−0.0102(5)	–	1.4(1)	1.8(2)	–
P(14)	−14	−0.0099(4)	−0.0098(4)	–	1.3(1)	1.4(1)	–
P(12)	−12	−0.0098(4)	−0.0101(5)	–	2.1(2)	1.6(2)	–
P(10)	−10	−0.0095(4)	−0.0094(4)	–	1.5(2)	1.7(2)	–
P(8)	−8	−0.0100(4)	−0.0090(4)	–	1.5(2)	2.3(2)	–
P(6)	−6	−0.0074(3)	−0.0084(4)	–	1.3(1)	1.1(1)	–
P(4)	−4	−0.0070(3)	−0.0071(3)	–	1.7(2)	1.4(1)	–
P(2)	−2	−0.0064(3)	−0.0063(3)	–	1.7(2)	1.6(2)	–
P(1)	−1	−0.0059(3)	−0.0058(3)	–	1.7(2)	1.5(2)	–
R(0)	1	−0.0039(2)	−0.0039(2)	−0.0071(3)	0.4(0)	0.4(0)	1.7(2)
R(1)	2	−0.0058(3)	−0.0058(3)	−0.0072(3)	0.2(0)	0.1(0)	1.8(2)
R(2)	3	−0.0062(3)		−0.0072(3)	0.6(1)	0.6(1)	1.8(2)

(*continued*)

Downloaded by [University of Lethbridge] at 16:49 28 July 2015

Table 6. Continued.

Line	m	$\delta^0_{\mathrm{N2\ Voigt}}(296)$	$\delta^0_{\mathrm{N2\ hard}}(296)$	$\delta^0_{\mathrm{calc}}(296)$	$\delta'_{\mathrm{Voigt}} \times 105$	$\delta'_{\mathrm{hard}} \times 105$	$\delta'_{\mathrm{calc}} \times 105$
R(4)	5	−0.0063(3)	−0.0063(3)	−0.0074(3)	0.9(1)	0.9(1)	2.3(2)
R(6)	7	−0.0064(3)	−0.0065(3)	−0.0081(4)	0.7(1)	0.7(1)	2.9(3)
R(8)	9	−0.0075(3)	−0.0075(3)	−0.0087(4)	0.7(1)	0.7(1)	3.0(3)
R(10)	11	−0.0080(4)	−0.0086(4)	−0.009(4)	0.9(1)	0.9(1)	3.0(3)
R(12)	13	−0.0092(4)	−0.0092(4)	−0.0091(4)	1.9(2)	1.9(2)	3.0(3)
R(14)	15	−0.0098(4)	−0.0098(4)	−0.0092(4)	2.7(3)	2.3(2)	3.3(3)
R(16)	17	−0.0106(5)	−0.0106(5)	−0.0095(4)	3.7(4)	3.7(4)	3.7(4)
R(18)	19	−0.0111(5)	−0.0111(5)	−0.0099(4)	4.1(4)	4.0(4)	4.2(4)
R(20)	21	−0.0111(5)	−0.0111(5)	−0.0105(5)	4.4(4)	4.4(4)	4.8(5)
R(21)	22	−0.0119(5)	−0.0118(5)	−0.0108(5)	3.9(4)	3.9(4)	5.1(5)
R(22)	23	−0.0121(5)	−0.0120(5)	−0.0111(5)	4.4(4)	4.5(5)	5.4(5)
R(23)	24	−0.0124(6)	−0.0124(6)	−0.0114(5)	4.2(4)	4.2(4)	5.7(6)
R(24)	25	−0.0123(6)	−0.0123(6)	−0.0117(5)	4.5(5)	4.5(5)	5.9(6)
R(25)	26	−0.0124(6)	−0.0123(6)	−0.012(5)	5.2(5)	5.4(5)	6.2(6)
R(26)	27	−0.0126(6)	−0.0129(6)	−0.0124(6)	4.7(5)	5.3(5)	6.4(6)
R(27)	28	−0.0132(6)	−0.0132(6)	−0.0127(6)	4.8(5)	4.8(5)	6.6(7)
R(28)	29	−0.0130(6)	−0.0132(6)	−0.013(6)	4.6(5)	5.4(5)	6.8(7)
R(29)	30	−0.0139(6)	−0.0139(6)	−0.0133(6)	4.2(4)	4.3(4)	7.0(7)
R(30)	31	−0.0133(6)	−0.0133(6)	−0.0137(6)	4.8(5)	4.9(5)	7.2(7)
R(31)	32	−0.0138(6)	−0.0138(6)	−0.014(6)	4.4(4)	4.4(4)	7.4(7)
R(32)	33	−0.0133(6)	−0.0133(6)	−0.0143(6)	4.6(5)	3.1(3)	7.5(8)
R(33)	34	−0.0140(6)	−0.0140(6)	−0.0146(7)	4.5(5)	4.5(5)	7.7(8)

Table 7. N_2-shifting coefficients δ^0_{N2} ($cm^{-1}\,atm^{-1}$) at 296 K and their temperature dependence parameters δ'_{1N2} and δ'_{2N2} (according to Equation 4). The experimental results are derived from measurements assuming the Voigt and hard-collision lineshapes (values quoted in parentheses correspond to one standard deviation). The theoretical values are calculated for the *R*-branch only (except very low *m*-values, shifts in the *P*- and *R*-branches are symmetric).

Lines	m	$\delta^0_{\mathrm{N2\ Voigt}}$ (296)	$\delta^0_{\mathrm{N2\ hard}}$ (296)	$\delta^0_{\mathrm{N2\ calc}}$ (296)	$\delta'_{\mathrm{1N2\ Voigt}} \times 10^5$	$\delta'_{\mathrm{1N2\ hard}} \times 10^5$	$\delta'_{\mathrm{1N2\ calc}} \times 10^5$	$\delta'_{\mathrm{2N2\ Voigt}} \times 10^7$	$\delta'_{\mathrm{2N2\ hard}} \times 10^7$	$\delta'_{\mathrm{2N2\ calc}} \times 10^7$
P(31)	−31	−0.0121(5)	−0.0118(5)	–	0.87(9)	0.37(4)		−0.94(1)	−1.47(1)	
P(30)	−30	−0.0104(5)	−0.0107(5)	–	–3.66(37)	−3.14(31)		−1.93(2)	−15.37(15)	
P(29)	−29	−0.0118(5)	−0.0122(6)	–	0.21(2)	0.21(2)		−1.36(1)	−1.44(1)	
P(28)	−28	−0.0109(5)	−0.0119(5)	–	3.00(30)	−1.18(12)		−0.65(1)	−1.90(2)	
P(27)	−27	−0.0115(5)	−0.0112(5)	–	0.37(4)	0.34(3)		−0.14(0)	−2.43(2)	
P(26)	−26	−0.0110(5)	−0.0117(5)	–	0.94(9)	0.31(3)		−1.12(1)	−1.07(1)	
P(25)	−25	−0.0117(5)	−0.0114(5)	–	1.26(13)	1.14(11)		−0.03(0)	0.53(1)	
P(24)	−24	−0.0108(5)	−0.0108(5)	–	0.85(8)	1.21(12)		−0.97(1)	−0.57(1)	
P(23)	−23	−0.0113(5)	−0.0105(5)	–	1.15(12)	1.90(19)		0.55(1)	−4.31(4)	
P(22)	−22	−0.0111(5)	−0.0105(5)	–	0.44(4)	0.99(10)		0.65(1)	−1.14(1)	
P(21)	−21	−0.0114(5)	−0.0110(5)	–	−0.42(4)	1.64(16)		0.63(1)	−0.06(0)	
P(20)	−20	−0.0105(5)	−0.0107(5)	–	1.15(12)	0.82(8)		0.30(0)	0.040(0)	
P(18)	−18	−0.0128(6)	−0.0121(5)	–	4.31(43)	−0.95(9)		0.37(0)	−0.49(0)	
P(16)	−16	−0.0106(5)	−0.0100(5)	–	2.63(26)	1.50(15)		2.75(3)	−0.98(1)	
P(14)	−14	−0.0101(5)	−0.0101(5)	–	5.49(55)	5.33(53)		1.88(2)	8.61(9)	
P(12)	−12	−0.0098(4)	−0.0101(5)	–	3.60(36)	3.31(33)		1.45(1)	2.55(3)	
P(10)	−10	−0.0092(4)	−0.0095(4)	–	4.84(48)	3.43(34)		0.82(1)	3.71(4)	
P(8)	−8	−0.0096(4)	−0.0090(4)	–	10.85(19)	3.53(35)		2.03(2)	1.82(2)	
P(6)	−6	−0.0075(3)	−0.0951(43)	–	1.70(17)	5.95(60)		11.16(11)	10.53(11)	
P(4)	−4	−0.0070(3)	−0.0071(3)	–	3.07(31)	1.39(14)		−0.17(0)	−0.11(0)	
P(2)	−2	−0.0064(3)	−0.0025(1)	–	1.68(17)	1.23(12)		−0.01(0)	−0.81(1)	
P(1)	−1	−0.0056(3)	−0.0051(2)	–	0.38(4)	−1.1(11)		−2.90(3)	−5.04(5)	
R(0)	1	−0.0035(2)	−0.0035(2)	−0.0071	−1.45(15)	−1.47(15)	1.54	−4.09(4)	−4.07(4)	−0.37
R(1)	2	−0.0057(3)	−0.0056(3)	−0.0072	−0.56(6)	−0.70(7)	1.57	−1.60(2)	−1.74(2)	−0.43
R(2)	3	−0.0062(3)		−0.0071	0.49(5)	0.49(5)	1.60	−0.28(0)	−0.28(0)	−0.50
R(4)	5	−0.0067(3)	−0.0066(3)	−0.0073	2.03(20)	1.89(19)	1.93	5.00(5)	3.66(4)	−0.77

(*continued*)

Downloaded by [University of Lethbridge] at 16:49 28 July 2015

Table 7. Continued.

Lines	m	$\delta^0_{N2\ Voigt}$ (296)	$\delta^0_{N2\ hard}$ (296)	$\delta^0_{N2\ calc}$ (296)	$\delta'_{1N2\ Voigt} \times 10^5$	$\delta'_{1N2\ hard} \times 10^5$	$\delta'_{1N2\ calc} \times 10^5$	$\delta'_{2N2\ Voigt} \times 10^7$	$\delta'_{2N2\ hard} \times 10^7$	$\delta'_{2N2\ calc} \times 10^7$
R(6)	7	−0.0063(3)	−0.0065(3)	−0.0080	0.69(7)	0.73(7)	2.43	0.40(0)	0.27(0)	−0.97
R(8)	9	−0.0079(4)	−0.0079(4)	−0.0086	2.34(23)	2.28(23)	2.62	3.48(3)	3.49(3)	−0.90
R(10)	11	−0.0082(4)	−0.0098(4)	−0.0089	1.82(18)	1.93(19)	2.56	3.02(3)	15.76(16)	−0.86
R(12)	13	−0.0093(4)	−0.0093(4)	−0.0090	2.40(24)	2.39(24)	2.58	1.04(1)	1.02(1)	−0.98
R(14)	15	−0.0098(4)	−0.0099(4)	−0.0091	2.53(25)	2.67(27)	2.74	0.37(0)	0.91(1)	−1.21
R(16)	17	−0.0106(5)	−0.0106(5)	−0.0094	3.60(36)	3.57(36)	3.03	−0.25(0)	−0.31(0)	−1.51
R(18)	19	−0.0110(5)	−0.0110(5)	−0.0097	3.50(35)	3.40(34)	3.41	−1.28(1)	−1.42(1)	−1.82
R(20)	21	−0.0110(5)	−0.0110(5)	−0.0102	3.93(39)	3.84(38)	3.83	−1.07(1)	−1.25(1)	−2.13
R(21)	22	−0.0182(8)	−0.0118(5)	−0.0105	3.80(38)	3.77(38)	4.05	−0.31(0)	−0.36(0)	−2.27
R(22)	23	−0.0118(5)	−0.0117(5)	−0.0108	3.08(31)	3.09(31)	4.27	−2.87(3)	−3.05(3)	−2.41
R(23)	24	−0.0122(5)	−0.0122(5)	−0.0111	3.33(33)	3.33(33)	4.49	−1.97(2)	−1.99(2)	−2.53
R(24)	25	−0.0124(6)	−0.0124(6)	−0.0114	4.74(47)	4.72(47)	4.70	0.43(0)	0.40(0)	−2.64
R(25)	26	−0.0124(6)	−0.0123(6)	−0.0117	5.43(54)	5.39(54)	4.90	0.18(0)	0.07(0)	−2.74
R(26)	27	−0.0129(6)	−0.0127(6)	−0.0121	4.55(45)	4.46(45)	5.09	−1.63(2)	−1.78(2)	−2.84
R(27)	28	−0.0130(6)	−0.0130(6)	−0.0124	4.06(41)	4.07(41)	5.28	1.54(2)	−1.57(2)	−2.91
R(28)	29	−0.0129(6)	−0.0132(6)	−0.0127	5.33(53)	5.36(54)	5.45	−0.09(0)	−0.02(0)	−2.99
R(29)	30	−0.0137(6)	−0.0137(6)	−0.0130	3.32(33)	3.35(33)	5.62	−1.97(2)	−1.99(2)	−3.04
R(30)	31	−0.0131(6)	−0.0131(6)	−0.0133	4.02(40)	4.05(41)	5.77	−1.79(2)	−1.75(2)	−3.11
R(31)	32	−0.0138(6)	−0.0137(6)	−0.0136	4.3(43)	4.18(42)	5.92	−0.25(0)	−0.48(0)	−3.15
R(32)	33	−0.0132(6)	−0.0132(6)	−0.0139	4.27(43)	4.49(45)	6.06	4.61(5)	−1.36(1)	−3.22
R(33)	34	−0.0140(6)	−0.0140(6)	−0.0142	4.55(45)	4.59(46)	6.19	0.15(0)	0.10(0)	−3.26

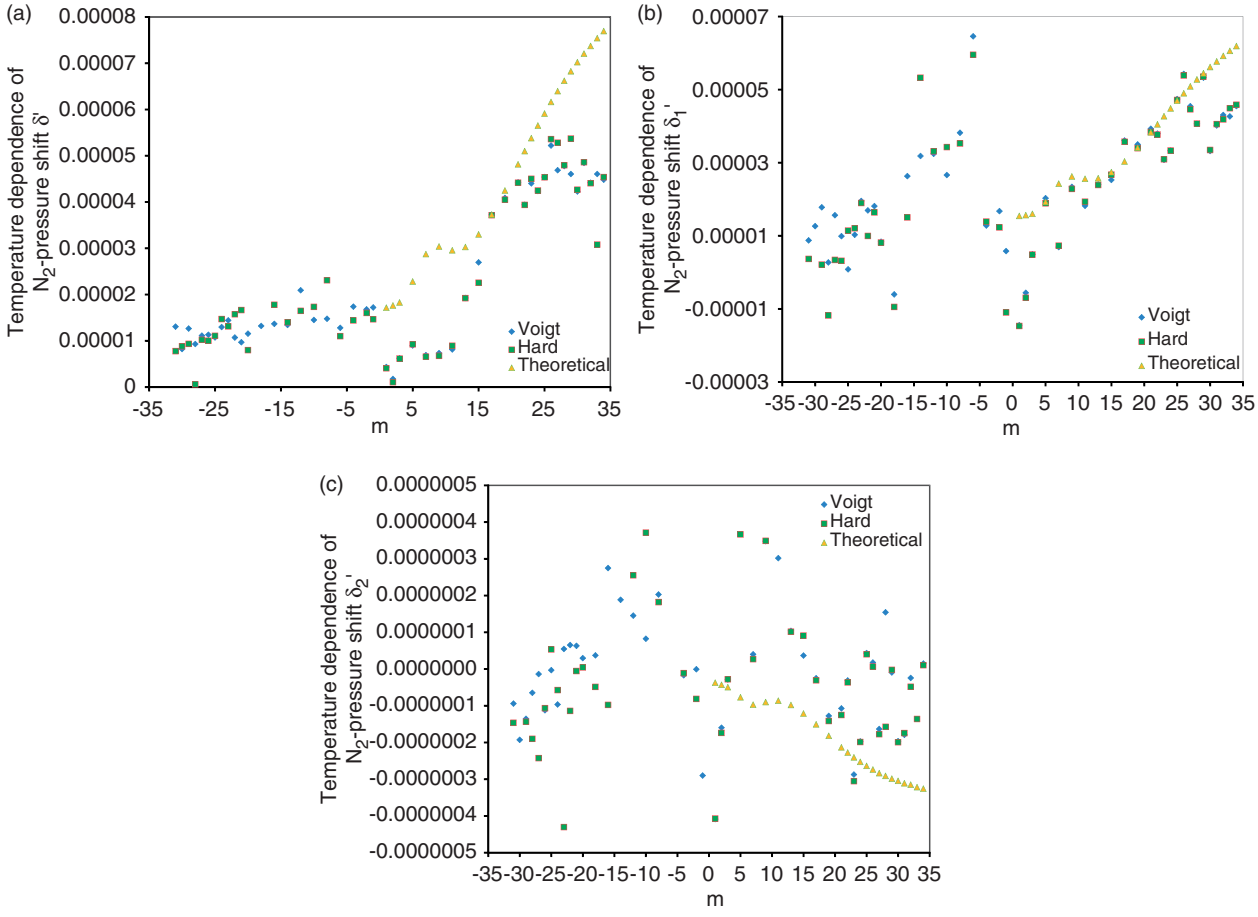

Figure 8. Temperature-dependence terms of N_2-shifts of C_2H_2 transitions: (A) δ' obtained from Equation (3), (B) δ_1' obtained from equation (4), and (C) δ_2' obtained from Equation (4).

Downloaded by [University of Lethbridge] at 16:49 28 July 2015

temperature exponents, n, for the broadening coefficients as well as the temperature-dependence characteristics for the pressure-shift coefficients.

The experimental results have been supported by semiclassical calculations of Robert–Bonamy type with exact trajectories. A good agreement has been stated between our calculations and measurements.

Acknowledgements

This work was supported by the Natural Sciences and Engineering Research Council of Canada.

Note

1. For a fixed σ-value, decreasing of the potential depth ε results in an overall downward translation of the theoretical curve for the line widths, so that we have not modified the initial ε-value.

References

[1] R.A. Hanel, B.J. Conrath, D.E. Jennings and R.E. Samuelson, *Exploration of the Solar System by Infrared Remote Sensing* (Cambridge University Press, Cambridge, 1992).
[2] V.M. Devi, D.C. Benner, C.P. Rinsland, M.A.H. Smith and B.D. Sidney, J. Mol. Spectrosc. **114**, 49 (1985).
[3] D. Lambot, G. Blanquet and J.P. Bouanich, J. Mol. Spectrosc. **136**, 86 (1989).
[4] J.P. Bouanich, D. Lambot, G. Blanquet and J. Walrand, J. Mol. Spectrosc. **140**, 195 (1990).
[5] P. Varanasi, J. Quant. Spectrosc. Radiat. Transfer **47**, 263 (1992).
[6] A.S. Pine, J. Quant. Spectrosc. Radiat. Transfer **50**, 149 (1993).
[7] A. Babay, M. Ibrahimi, V. Lemaire, B. Lemoine, F. Rohart and J.P. Bouanich, J. Quant. Spectrosc. Radiat. Transfer **59**, 195 (1998).
[8] J.P. Bouanich, G. Blanquet, J.C. Populaire and J. Walrand, J. Mol. Spectrosc. **190**, 7 (1998).
[9] J.P. Bouanich, G. Blanquet and J. Walrand, J. Mol. Spectrosc. **203**, 41 (2000).
[10] G. Blanquet, J. Walrand and J.P. Bouanich, J. Mol. Spectrosc. **210**, 1 (2001).
[11] H. Valipour and D. Zimmermann, J Chem Phys **114**, 3535 (2001).
[12] S.W. Arteaga, C.M. Bejger, J.L. Gerecke, J.L. Hardwick, Z.T. Martin, J. Mayo, E.A. McIlhattan, J.-M.F. Moreau, M.J. Pilkenton, M.J. Polston, B.T. Robertson and E.N. Wolf, J. Mol. Spectrosc. **243**, 253 (2007).
[13] M. Dhyne, L. Fissiaux, J.C. Populaire and M. Lepère, J. Quant. Spectrosc. Radiat. Transfer **110**, 358 (2009).
[14] L. Fissiaux, M. Dhyne and M. Lepère, J. Mol. Spectrosc. **254**, 10 (2009).
[15] M. Dhyne, P. Joubert, J.C. Populaire and M. Lepère, J. Quant. Spectrosc. Radiat. Transfer **111**, 973 (2010).
[16] C.P. McRaven, M.J. Cich, G.V. Lopez, T.J. Sears, D.R. Hurtmans and A.W. Mantz, J. Mol. Spectrosc. **266**, 43 (2011).
[17] C. Povey, A. Predoi-Cross and D.R. Hurtmans, J. Mol. Spectrosc. **268**, 177 (2011).
[18] N.T. Champbell, J.D. Cook, B.A. Coombs, E.P. Fuller, J.L. Hardwick, S.M. Hurley, L.K. Ho, P.A. Kovac, E.J. Robertson, E.N. Senning, J.K. Utterback and R.S. Wiser, Mol. Phys. **109**, 2199 (2011).
[19] P. Minutolo, C. Corsi, F.D. Amato and M. De Rosa, Eur. Phys. J. D **17**, 175 (2001).
[20] S.V. Ivanov, L. Nguyen and J. Buldyreva, J. Mol. Spectrosc. **233**, 60 (2005).
[21] J. Buldyreva, S.V. Ivanov and L. Nguyen, J. Raman Spectrosc. **36**, 148 (2005).
[22] L. Nguyen, S. Ivanov, O.G. Buzykin and J. Buldyreva, J. Mol. Spectrosc. **239**, 101 (2006).
[23] J. Buldyreva and L. Nguyen, Mol. Phys. **102**, 1523 (2004).
[24] D. Hurtmans, G. Dufour, W. Bell, A. Henry, A. Valentin and C. Camy-Peyret, J. Mol. Spectrosc. **215**, 128 (2002).
[25] C. Povey, A. Predoi-Cross, D. Hurtmans, Mol. Phys., present issue.
[26] L.S. Rothman, I.E. Gordon, A. Barbe, D. Chris Benner, P.F. Bernath, M. Birk, V. Boudon, L.R. Brown, A. Campargue, J.-P. Champion, K. Chance, L.H. Coudert, V. Dana, V.M. Devi, S. Fally, J.-M. Flaud, R.R. Gamache, A. Goldman, D. Jacquemart, I. Kleiner, N. Lacome, W.J. Lafferty, J.-Y. Mandin, S.T. Massie, S. Mikhailenko, C.E. Miller, N. Moazzen-Ahmadi, O.V. Naumenko, A. Nikitin, J. Orphal, A. Predoi-Cross, V. Perevalov, A. Perrin, C.P. Rinsland, M. Rotger, M. Šimečková, M.A.H. Smith, K. Sung, S. Tashkun, J. Tennyson, R.A. Toth, A.C. Vandaele and J. Vander Auwera, J. Quant. Spectrosc. Radiat. Transfer **110**, 533 (2009).
[27] D. Robert and J. Bonamy, J. Phys. (Paris) **40**, 923 (1979).
[28] L.D. Landau and E.M. Lifshits, *Course of Theoretical Physics v.1 Mechanics* (Pergamon, Oxford, 1976).
[29] F. Thibault, B. Corretja, A. Viel, D. Bermejo, R.Z. Martinez and B. Bussery-Honvault, Phys. Chem. Chem. Phys. **10**, 5419 (2008).
[30] J. Buldyreva and L. Nguyen, Phys. Rev. A **77**, 042720 (2008).
[31] D.E. Stogryn and A.P. Stogryn, Mol. Phys. **11**, 371 (1966).
[32] H. Yasuda and T. Yamamoto, Prog. Theor. Phys. **45**, 1458 (1971).
[33] J. Buldyreva, J. Bonamy, M.C. Weikl, F. Beyrau, T. Seeger, A. Leipertz, F. Vestin, M. Afzelius, J. Bood and P.E. Bengtsson, J. Ram. Spectrosc. **37**, 647 (2006).
[34] D. Jacquemart, A. Laraia, F. Kwabia Tchana, R.R. Gamache, A. Perrin and N. Lacôme, J. Quant. Spectrosc. Radiat. Transfer **111**, 1209 (2010).
[35] W.H. Flygare and R.C. Benson, Mol. Phys. **20**, 225 (1971).
[36] J.P. Bouanich and A. Predoi-Cross, Mol. Phys. **109**, 2071 (2011).

Downloaded by [University of Lethbridge] at 16:49 28 July 2015